(currently University of Toyama) (#2004-47) and the ARVO Statement on the Use of Animals in Ophthalmic and Vision Research.

2.2. Reagents

[Estradiol-6, 7-^{3}H(N)]-estradiol 17β-D-glucuronide ([^{3}H]E17βG, 45 Ci/mmol) and D-[1-^{14}C]-mannitol ([^{14}C]D-mannitol, 51 mCi/mmol) were purchased from Perkin-Elmer Life Sciences (Boston, MA). All other chemicals were of reagent grade and available commercially.

2.3. Theory

The diffusion-flow model for drug transfer through a microdialysis probe from the vitreous chamber is illustrated in Fig. 2. The membrane portion of the device containing the unstirred water layer in the vitreous humor is regarded as a membrane of thickness L_M in which diffusion occurs in the x-direction. Thus, the flow of a drug in the membrane is given as

$$\frac{\partial C_M(t,x,z)}{\partial t} = D\frac{\partial^2 C_M(t,x,z)}{\partial x^2} \quad (1)$$

The initial condition of the equation is written as

$$t = 0, \quad C_M(t,x,z) = 0 \quad (2)$$

And the boundary conditions are as follows:

$$\text{(i)}\ x = 0, \quad C_M(t,x,z) = \varepsilon C_V(t) \quad (3)$$

$$\text{(ii)}\ x = L_M, \quad C_M(t,x,z) = \varepsilon C_T(t,z) \quad (4)$$

However, movement of drug in the tube portion of the device occurs through convective flow in the z-direction and diffusion through the membrane wall and the mass transfer equation is given as

$$\frac{\partial C_T(t,z)}{\partial t} = -v_Z\frac{\partial C_T(t,z)}{\partial z} - \frac{AD}{V}\left[\frac{\partial C_M(t,x,z)}{\partial x}\right]_{x=L_M} \quad (5)$$

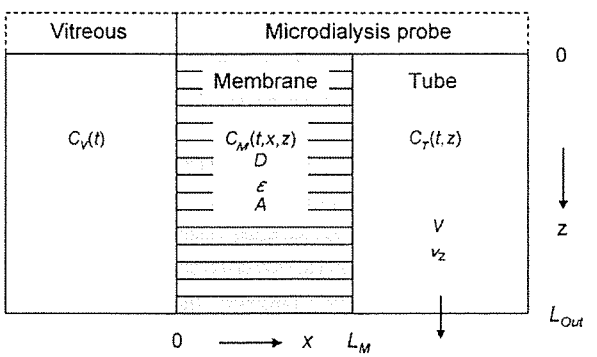

Fig. 2. Drug distribution between the microdialysis probe and the vitreous humor. C_V, concentration in the vitreous humor; C_M, concentration in the cellulose membrane; C_T, concentration in the tube; D, diffusion coefficient; ε, porosity; A, surface area; V, volume of the tube; v_Z, velocity of dialysate; L_M, membrane thickness; x, x-direction; z, z-direction; L_{out}, length between the tube inlet and outlet. v_Z and L_{out} were set at 6.37 cm/min and 2.0 mm, respectively.

The tube has an initial condition as follows:

$$t = 0, \quad C_T(t,z) = 0 \quad (6)$$

When the following variables are defined to simplify the solution, diffusion parameter: $D' = D/L_M^2$; partition parameter: $K' = \varepsilon L_M$; $d = \sqrt{s/D'}$; $\rho = A/V$, the Laplace transform of the outlet concentration of the microdialysis tube is given by (Appendix A)

$$\bar{C}_T(s, L_{out}) = \frac{\rho K'\bar{C}_V(s)}{\rho K'\cosh(d) + d\sinh(d)} \times \left\{1 - \exp\left[-s\left(1 + \frac{\rho K'}{d\tanh(d)}\right)\frac{L_{out}}{v_Z}\right]\right\} \quad (7)$$

2.3.1. When the concentration of the vitreous humor is constant

If the drug concentration in the vitreous humor has a constant value, i.e., $C_V(t) = C_0$, Eq. (7) can be rewritten and drug concentration profile in the outlet is given by

$$\bar{C}_T(s, L_{out}) = \frac{\rho K' C_0}{s[\rho K'\cosh(d) + d\sinh(d)]} \times \left\{1 - \exp\left[-s\left(1 + \frac{\rho K'}{d\tanh(d)}\right)\frac{L_{out}}{v_Z}\right]\right\} \quad (8)$$

By using the final-value theorem, the outlet concentration in the tube under steady-state conditions is given as

$$\lim_{t\to\infty} C_T(t, L_{out}) = \lim_{s\to 0} s\bar{C}_T(s, L_{out}) = C_0\left[1 - \exp\left(-\rho K' D'\frac{L_{out}}{v_Z}\right)\right] \quad (9)$$

2.3.2. When the concentration in the vitreous humor decays exponentially

If the drug concentration in the vitreous humor decreases in a mono-exponential fashion, i.e., $C_V(t) = C_0\exp(-\lambda_Z t)$, $C_T(t, L_{out})$ can be expressed by multi-exponential decay kinetics as follows (see Appendix B):

$$C_T(t, L_{out}) = U_Z\exp(-\lambda_Z t) + \sum_{n=1}^{n} U_n\exp(-D'\alpha_n^2 t) \quad (10)$$

where U_Z and U_n are given in Appendix B. Values for α_n are the roots of the following function:

$$\alpha_n\tan\alpha_n = \rho K' \quad (11)$$

Although Eq. (11) gives an infinite solution set, a single and minimum solution, α_1 exists in the region $[0, \pi/2]$. According to Eq. (10), if λ_Z is smaller than $D'\alpha_1^2$, the slope of drug concentration–time profiles in the outlet of the tube at a late time should be the same as that of the vitreous humor. However, if λ_Z is larger than $D'\alpha_1^2$ in which membrane transport is rate-limiting, the proportional relationship between both concentrations will no longer hold.

2.4. Microdialysis study

The rats were anesthetized with an intraperitoneal injection of ketamine–xylazine (60 mg/kg ketamine and 15 mg/kg xylazine) and their heads were mounted on a stereotaxic frame (SR-6, Narishige, Tokyo, Japan). Their eyelids were locally anesthetized by instillation of 2% xylocaine and fixed using surgical sutures in order not to blink. A 25-gauge needle was inserted about 1 mm below the corneal scleral limbus through the pars plana at a depth of 3.0 mm. The needle was removed and [^{3}H]E17βG (5 μCi) and [^{14}C]D-mannitol (1 μCi) dissolved in 1.0 μL Ringer-HEPES solution (141 mM NaCl, 4.0 mM KCl, 2.8 mM $CaCl_2$, 10.0 mM HEPES, pH 7.4) was administered using a 10 μL microsyringe (Hamilton, Reno, NE) at a depth of 3.0 mm from the surface of the eye. The microdialysis probe was implanted immediately into the vitreous chamber and fixed with surgical glue (Aron Alpha A, Sankyo, Tokyo) on the surface of the eye. The custom-designed microdialysis probe (TEP-50, Fig. 1B) was constructed by Eicom (Kyoto, Japan). The length of the tubing (cellulose membrane) was 2.0 mm and the molecular cutoff for the dialysis tubing was 50 kDa. Ringer-HEPES solution at 37 °C was delivered to the probe continuously at 2 μL/min via polyethylene tubing (SP19, inner diameter 0.35 mm, outer diameter 1.05 mm, Natsume, Tokyo, Japan) connected to an infusion pump (model 11, Harvard, Holliston, MA). The dialysate was collected at 10 min intervals in vials over a period of 5 h, and the radioactivity in each fraction was determined by liquid scintillation counting.

For the experiment conducted in the presence of inhibitors, each inhibitor was dissolved in Ringer-HEPES solution and delivered to the probe as described above. The retinas were isolated at different time-intervals and the concentration of E17βG, probenecid, *p*-aminohippuric acid (PAH), sulfobromophthalein (BSP), and dehydroepiandrosterone sulfate (DHEAS) in the retina was determined by high-performance liquid chromatography (HPLC) using a 4.6 mm × 15 mm Inertsil ODS-2^{TM} column (GL Sciences, Tokyo, Japan) and a UV monitor. The concentration of digoxin in the retina was determined using a kit (TDX^{TM}-digoxin, Abbott Japan, Tokyo, Japan). The plateau concentration of inhibitors in the retina was reached within 1 h.

The probe recovery was assessed in the in vitro medium containing a constant level of compounds and calculated as

$$\text{recovery}\,(\%) = \frac{C_T}{C_V} \times 100 \tag{12}$$

where C_T (dpm/mL) is concentration of dialysate solution and C_V (dpm/mL) is the concentration in the test solution or isolated vitreous humor. The vitreous humor was isolated and pre-equilibrated with test solution for 2 h. The parameters, D' and $\rho K'$, were estimated using Eq. (8) with the non-linear least squares program MULTI (FILT) (Yano et al., 1989). We used a lag-time of 6 min for the passage through the polyethylene tubing connected to the distal end of the microdialysis probe. The recovery of [^{3}H]E17βG from the solution and vitreous humor was 3.51 ± 0.10% and 2.97 ± 0.09%, respectively. The recovery of [^{14}C]D-mannitol from the solution and vitreous humor was 3.96 ± 0.10% and 3.62 ± 0.16%, respectively. The recovery ratio from the solution and vitreous humor for [^{3}H]E17βG and [^{14}C]D-mannitol was 85% and 91%, respectively. The recovery of the probe in the vitreous chamber did not differ markedly from that in the test solution. The predicted values of D' for [^{3}H]E17βG and [^{14}C]D-mannitol in the vitreous preparation (mean ± S.E.M., $n = 3$) were 0.123 ± 0.007 and 0.127 ± 0.010 min^{-1}, respectively. The corresponding $\rho K'$ values for [^{3}H]E17βG and [^{14}C]D-mannitol were 7.72 ± 0.48 and 8.99 ± 0.74, respectively. Thus, the rate constant, $D'\alpha_1^2$ was expected to be within the range 0.3–0.4 min^{-1} for both compounds. The value was much larger than that obtained for the in vivo terminal phase (see Section 3), suggesting that the transport across the microdialysis probe is not the rate-limiting step in vivo.

2.5. Determination of elimination profile after intravitreal injection

The vitreous concentrations normalized by the injected dose (C_P (% dose/mL)), were estimated from the radioactivities in the dialysate using Eq. (13) and the C_P at time t, $C_p(t)$ was fitted to a bi-exponential equation (Eq. (14)) by non-linear least squares regression analysis using the computer program MULTI (Yamaoka et al., 1981):

$$C_p = \frac{C_T}{\text{Dose}_{\text{tracer}}} \times 100 \tag{13}$$

$$C_p(t) = A\,e^{-\alpha t} + B\,e^{-\beta t} \tag{14}$$

where C_T is the concentration in the dialysate (dpm/mL) and $\text{Dose}_{\text{tracer}}$ (dpm) is the total radioactivity of substance after intravitreal injection. The constants A and B are intercepts on the y-axis for each exponential segment of the curve in Eq. (14). The constants α and β are the apparent first-order rate constants for the initial and terminal phase, respectively. The pharmacokinetic parameters (A, α, B, and β) were successfully estimated by the damping Gauss–Newton method.

Unless otherwise indicated, all data represent means ± S.E.M. An unpaired, two-tailed Student's t-test was used to determine the significance of differences between two group means. Statistical significance of differences among means of several groups was determined by one-way analysis of variance (ANOVA) followed by the modified Fisher's least squares difference method.

3. Results

3.1. Elimination of [^{3}H]E17βG from the vitreous humor in vivo

Fig. 3A shows a typical elimination curve of [^{3}H]E17βG and [^{14}C]D-mannitol from the vitreous humor after bolus injection. [^{3}H]E17βG and [^{14}C]D-mannitol were bi-exponentially eliminated from the vitreous humor. Although the first rapid decline was almost the same for both compounds, the second decline in [^{3}H]E17βG was significantly greater than that of [^{14}C]D-mannitol (Fig. 3A). The elimination rate constant (β) of [^{3}H]E17βG during the terminal phase was 9.32 ± 0.83 × 10^{-3} min^{-1} ($n = 5$), which was 1.9-fold greater

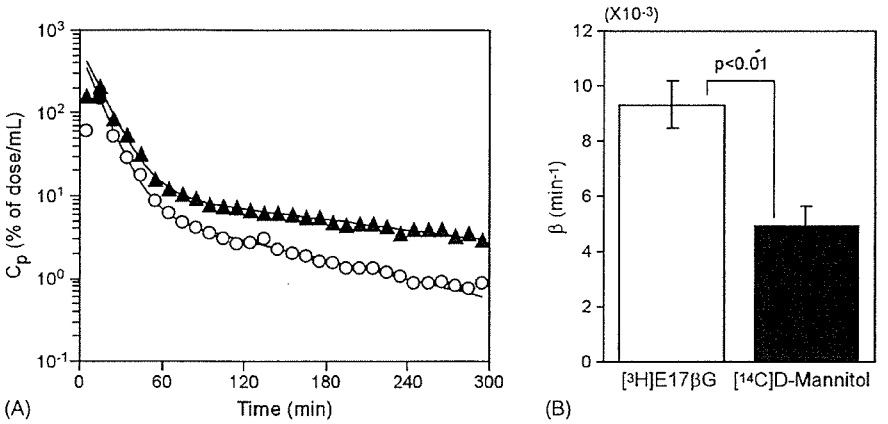

Fig. 3. Typical outflow pattern of [^{3}H]E17βG and [^{14}C]D-mannitol from the microdialysis probe (A) and elimination rate constants (β) of [^{3}H]E17βG and [^{14}C]D-mannitol during the terminal phase (B). Closed triangles and open circles represent the concentration in dialysate of [^{14}C]D-mannitol and [^{3}H]E17βG, respectively (A). Each column represents the mean ± S.E.M. ($n = 5$) (B).

than that of [^{14}C]D-mannitol ($4.97 \pm 0.69 \times 10^{-3}$ min^{-1}, $n = 5$) (Fig. 3B), supporting the hypothesis that elimination rate difference between [^{3}H]E17βG and [^{14}C]D-mannitol during the terminal phase involves efflux transport of [^{3}H]E17βG across the BRB.

3.2. Effect of several organic anions on the efflux transport of [^{3}H]E17βG

To examine whether the difference between the β-value of [^{3}H]E17βG and [^{14}C]D-mannitol contributes carrier-mediated efflux transport of E17βG, inhibition study was performed. The β-value of [^{3}H]E17βG was significantly reduced in the presence of 0.3 mM E17βG, 1.0 mM probenecid, 0.6 mM BSP, 0.1 mM DHEAS and 0.35 μM digoxin in the retina, whereas 0.7 mM PAH in the retina had no effect. On the other hand, the β-value of [^{14}C]D-mannitol was unchanged in the presence of all the inhibitors (Table 1), showing that inhibitors do not affect [^{14}C]D-mannitol transport. Fig. 4 shows the elimination rate differences between [^{3}H]E17βG and [^{14}C]D-mannitol during the terminal phase. In the presence of 0.3 mM E17βG in the retina, the efflux of [^{3}H]E17βG across the BRB was inhibited by 90.6%, suggesting that E17βG is transported via a carrier-mediated efflux transport process across the BRB. Moreover, 1.0 mM probenecid, and 0.6 mM BSP in the retina inhibited the efflux transport of [^{3}H]E17βG by 99.5% and 93.8%, respectively. DHEAS at 0.1 mM and digoxin at 0.35 μM in the retina reduced [^{3}H]E17βG efflux transport by 71.5% and 83.2%, respectively. In contrast, another organic anion, PAH at 0.7 mM, in the retina had no effect on [^{3}H]E17βG efflux transport.

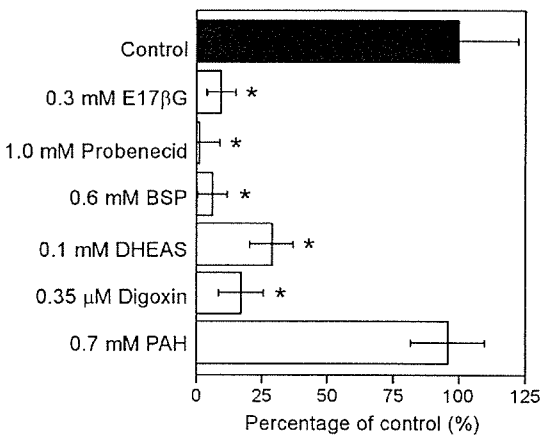

Fig. 4. Elimination rate difference between [^{3}H]E17βG and [^{14}C]D-mannitol during the terminal phase. Each column represents the mean ± S.E.M. ($n = 4$–6). $^*p < 0.01$, significantly different from the control. Percentage of control was calculated from data in Table 1 as follows: {β-value of [^{3}H]E17βG − β-value of [^{14}C]D-mannitol in the presence of inhibitor}/{β-value of [^{3}H]E17βG − β-value of [^{14}C]D-mannitol in the absence of inhibitor} × 100.

Table 1
Effect of inhibitors on elimination rate constants (β) of [^{3}H]E17βG and [^{14}C]D-mannitol during the terminal phase

Inhibitors (retinal concentration)	β (×10^{-3} min^{-1})	
	[^{3}H]E17βG	[^{14}C]D-Mannitol
Control	9.32 ± 0.08	4.97 ± 0.69
E17βG (0.3 mM)	6.62 ± 1.09*	6.21 ± 0.92
Probenecid (1.0 mM)	5.65 ± 0.64*	5.63 ± 1.01
BSP (0.6 mM)	5.87 ± 0.42*	5.60 ± 0.31
DHEAS (0.1 mM)	5.83 ± 0.36*	4.59 ± 0.23
Digoxin (0.35 μM)	6.03 ± 0.46*	5.30 ± 0.27
PAH (0.7 mM)	10.3 ± 0.91	6.14 ± 0.31

Each inhibitor was continuously perfused through the microdialysis probe which was implanted into the vitreous chamber. Concentration of inhibitors in the retina was determined by HPLC or a kit (digoxin). Each value represents the mean ± S.E.M. ($n = 4$–6). E17βG, estradiol 17-β glucuronide; BSP, sulfobromophthalein; DHEAS, dehydroepiandrosterone sulfate; PAH, *p*-aminohippuric acid.
* $p < 0.01$ significantly different from the control.

4. Discussion

The present study is the first time to demonstrate the efflux transport of E17βG across the rat BRB by the use of in vivo microdialysis. The dialysate concentration of [^{3}H]E17βG and [^{14}C]D-mannitol in the vitreous humor via the microdialysis probe decayed in a bi-exponential manner (Fig. 3A). The first

slope of the drug concentration–time profile was steeper than that of the second. This supports the hypothesis that the first and second declines reflect diffusion into the vitreous humor, including the microdialysis tube, after vitreous bolus injection and the elimination from the vitreous humor of both compounds, respectively. Therefore, Eq. (10) can be used to estimate the vitreous concentration of drug via the microdialysis probe and the β-value of [^{3}H]E17βG and [^{14}C]D-mannitol was estimated by non-linear least squares fitting of a bi-exponential equation (Eq. (14)) to the vitreous concentration values. The β-value of [^{3}H]E17βG was 1.9-fold greater than that of [^{14}C]D-mannitol, which is a bulk flow marker for passage from the vitreous humor to Schlemm's canal and/or the uveoscleral outflow route (Fig. 3B). This result supports the hypothesis that [^{3}H]E17βG undergoes efflux transport across the BRB in addition to elimination from the vitreous humor via bulk flow and passive diffusion (Fig. 1A). Macha and Mitra (2001) used two microdialysis probes implanted in the rabbit anterior and vitreous chambers to show that the vitreous concentration of fluorescein decayed bi-exponentially after bolus injection into the vitreous humor and fluorescein appeared in aqueous humor, showing that fluorescien is eliminated from the anterior chamber via Schlemm's canal and/or the uveoscleral outflow route as well as via the BRB. This was in good agreement with our results. Since we used [^{14}C]D-mannitol as a bulk flow marker, the vitreous humor/retina-to-blood efflux transport of E17βG can be used to estimate the difference in the elimination rate between [^{3}H]E17βG and [^{14}C]D-mannitol during the terminal phase even when there was a single microdialysis probe in the vitreous humor.

BRB damage due to the implantation of a microdialysis probe would affect the estimation of the BRB efflux transport, particularly in the case of small molecules. Using [^{14}C]D-mannitol, a very slow permeable marker of the BRB (Lightman et al., 1987), the β-value of [^{14}C]D-mannitol was almost constant even when inhibitors are present in the retina (Table 1). These results suggest that only limited physical damage to the BRB was caused by the implantation of a microdialysis probe in the vitreous chamber.

In order to discover whether an organic anion transport process is involved in the efflux transport of E17βG at the BRB, a microdialysis study was performed in the presence of several organic anions. In the presence of 0.3 mM E17βG in the retina, the β-value of [^{3}H]E17βG was significantly reduced by the level of [^{14}C]D-mannitol (Table 1), suggesting that E17βG is transported via a carrier-mediated efflux transport process across the BRB. [^{3}H]E17βG efflux transport from rat vitreous humor/retina was significantly inhibited by probenecid, BSP, and DHEAS, but not by PAH (Fig. 4). This inhibition pattern agrees well with that of the organic anion transporting polypeptide (Oatp) family rather than the organic anion transporter (OAT) family (Reichel et al., 1999; Sekine et al., 2000; Sugiyama et al., 2001). Although Oatp and OAT family are sensitive for probenecid, BSP, and DHEAS, Oatp is PAH-insensitive organic anion transporter (Reichel et al., 1999; Sekine et al., 2000; Sugiyama et al., 2001). Moreover, [^{3}H]E17βG efflux transport was significantly inhibited by digoxin at 0.35 μM (Fig. 4). Although digoxin is a specific substrate for Oatp1a4 (Slc21a5; Oatp2) and Oatp4c1 (Slco4c1; Oatp-H) with a Michaelis–Menten constant of 0.24 and 8.0 μM, respectively, Oatp1a4 has higher affinity of digoxin than that of Oatp4c1 (Hagenbuch and Meier, 2003; Mikkaichi et al., 2004; Noé et al., 1997). These findings suggest that Oatp1a4 is involved in vitreous humor/retina-to-blood efflux transport of E17βG at the BRB. Gao et al. (2002) provided morphological evidence using immunofluorescence confocal microscopy, showing that Oatp1a4 is localized on the apical side of rat RPE (outer BRB) and at the inner BRB. In the rat brain, Oatp1a4 is localized on both the luminal and abluminal sides of the blood–brain barrier (BBB) (Gao et al., 1999). Although localization of Oatp1a4 at the inner BRB has not yet been demonstrated, the localization of Oatp1a4 at the inner BRB may be similar to that of the BBB. Using a combination of a magnetic isolation method for rat retinal vascular endothelial cells and real-time quantitative PCR analysis, we found recently that Oatp1a4 and 1c1 (Slc21a14; Oatp14) mRNA are predominantly expressed at the inner BRB (Tomi and Hosoya, 2004). Oatp1c1 has been identified as a BBB-specific anion transporter which has E17βG as a substrate (Li et al., 2001; Sugiyama et al., 2003). However, Oatp1c1 does not have a high affinity for digoxin (50% inhibition concentration >0.5 mM) (Sugiyama et al., 2003). Taking these results into consideration, Oatp1a4 is at least partly involved in the uptake of E17βG from the retina in the vitreous humor/retina-to-blood efflux transport process. However, the transport system at the basolateral side of the RPE and the involvement of other organic anion transporters, such as multidrug resistance associated protein (MRP) and the OAT family, at the BRB are unclear and remain the subject of ongoing investigation.

In conclusion, the efflux transport of [^{3}H]E17βG across the rat BRB has been evaluated by application of a microdialysis probe to the vitreous humor. A functional in vivo inhibition study suggests that the BRB is involved in the efflux transport of E17βG, at least as far as Oatp1a4 is concerned. To the best of our knowledge, this is the first report to characterize the efflux transport of organic anions at the rat BRB in vivo. These findings provide important information about the physiological role of the BRB and how the BRB restricts amphipathic organic anions distribution to the retina.

Acknowledgements

The authors would like to thank Dr. Junichi Kawakami for valuable discussions. This study was supported, in part, by a Grant-in-Aid for Scientific Research from the Japan Society for the Promotion of Science and a grant for Research on Sensory and Communicative Disorders by the Ministry of Health, Labor, and Welfare, Japan.

Appendix A

We proposed the Laplace transforms $\bar{C}_V(s)$, $\bar{C}_M(s, x, z)$ and $\bar{C}_T(s, z)$ for the functions of time, $C_V(t)$, $C_M(t, x, z)$ and $C_T(t, z)$, respectively. The Laplace transformation of Eqs. (1) and (2)

is given as

$$s\bar{C}_M(s,x,z) = D\frac{\partial^2 \bar{C}_M(s,x,z)}{\partial x^2} \quad (A.1)$$

The general solution of Eq. (A.1) can be written as

$$\bar{C}_M(s,x,z) = A_1(z)\cosh\left(\sqrt{\frac{s}{D}}x\right) + A_2(z)\sinh\left(\sqrt{\frac{s}{D}}x\right) \quad (A.2)$$

The Laplace transforms corresponding to Eqs. (3) and (4) are:

$$\text{(i)}\ \bar{C}_M(s,0,z) = \varepsilon\bar{C}_V(s) \quad (A.3)$$

$$\text{(ii)}\ \bar{C}_M(s,L_M,z) = \varepsilon\bar{C}_T(s,z) \quad (A.4)$$

Substituting Eqs. (A.3) and (A.4) for (A.2) gives

$$A_1(z) = \varepsilon\bar{C}_V(s) \quad (A.5)$$

$$A_2(z) = \frac{\varepsilon}{\sinh(d)}[\bar{C}_T(s,z) - \bar{C}_V(s)\cosh(d)] \quad (A.6)$$

The equation corresponding to Eqs. (5) and (6) is

$$s\bar{C}_T(s,z) = -v_Z\frac{\partial \bar{C}_T(s,z)}{\partial z} - \rho D\left[\frac{\partial \bar{C}_M(s,x,z)}{\partial x}\right]_{x=L_M} \quad (A.7)$$

By rearranging Eq. (A.7), we obtain

$$v_Z\frac{\partial \bar{C}_T(s,z)}{\partial z} = -s\left[1 + \frac{\rho K'}{d\tanh(d)}\right]\bar{C}_T(s,z) + s\frac{\rho K'}{d\sinh(d)}\bar{C}_V(s) \quad (A.8)$$

Integrating from $z=0$ to L_{out}, we get

$$\bar{C}_T(s,L_{out}) = \frac{f_1(s)\bar{C}_V(s)}{g_1(s)}\left[1 - \exp\left(-\frac{sg_1(s)L_{out}}{v_Z}\right)\right] \quad (A.9)$$

where

$$f_1(s) = \frac{\rho K'}{d\sinh(d)} \quad (A.10)$$

$$g_1(s) = 1 + \frac{\rho K'}{d\tanh(d)} \quad (A.11)$$

Eq. (A.9) is identical to Eq. (7) in the text.

Appendix B

When the drug concentration in the vitreous humor decays exponentially, i.e., $C_V(t) = C_0\exp(-\lambda_Z t)$, $C_T(s,L_{out})$ is given as

$$\bar{C}_T(s,L_{out}) = \frac{f_2(s)}{g_2(s)} \quad (A.12)$$

where

$$f_2(s) = \rho K' C_0\left[1 - \exp\left(-\frac{sg_1(s)L_{out}}{v_Z}\right)\right] \quad (A.13)$$

$$g_2(s) = (s+\lambda_Z)[d\sinh(d) + \rho K'\cosh(d)] \quad (A.14)$$

Eq. (A.12) can be split into partial fractions as

$$\bar{C}_T(s,L_{out}) = \frac{U_Z}{s+\lambda_Z} + \sum_{n=1}^{n}\frac{U_n}{s+D'\alpha_n^2} \quad (A.15)$$

where

$$U_Z = \left[\frac{f_2(s)}{g_2'(s)}\right]_{S=-\lambda_Z} = \frac{\rho K' C_0\left\{1 - \exp\left[\left(1 - \frac{\rho K'}{\sqrt{\frac{\lambda_Z}{D'}}\tan\sqrt{\frac{\lambda_Z}{D'}}}\right)\frac{\lambda_Z L_{out}}{v_Z}\right]\right\}}{-\sqrt{\frac{\lambda_Z}{D'}}\sin\sqrt{\frac{\lambda_Z}{D'}} + \rho K'\cos\sqrt{\frac{\lambda_Z}{D'}}} \quad (A.16)$$

$$U_n = \left[\frac{f_2(s)}{g_2'(s)}\right]_{S=-D'\alpha_n^2} = \frac{2\rho K' D'\alpha_n C_0\left\{1 - \exp\left[\left(1 - \frac{\rho K'}{\alpha_n\tan\alpha_n}\right)\frac{D'\alpha_n^2 L_{out}}{v_Z}\right]\right\}}{(D'\alpha_n^2 - \lambda_Z)[(1+\rho K')\sin\alpha_n + \alpha_n\cos\alpha_n]} \quad (A.17)$$

The α_ns are the roots of:

$$\alpha_n\tan\alpha_n = \rho K' \quad (A.18)$$

The inverse Laplace transform of Eq. (A.15) is reduced to Eq. (10) in the text.

References

Alm A, Törnquist P. The uptake index method applied to studies on the blood–retinal barrier. Acta Physiol Scand 1981;113:73–9.

Anand BS, Atluri H, Mitra AK. Validation of an ocular microdialysis technique in rabbits with permanently implanted vitreous probes: systemic and intravitreal pharmacokinetics of fluorescein. Int J Pharm 2004;281:79–88.

BenEzra D, Maftzir G. Ocular penetration of cyclosporin A. The rabbit eye. Invest Ophthalmol Vis Sci 1990;31:1362–6.

Cunha-Vaz JG. The blood–retinal barriers system. Basic concepts and clinical evaluation. Exp Eye Res 2004;78:715–21.

Cunha-Vaz JG, Maurice D. Fluorescein dynamics in the eye. Doc Ophthalmol 1969;26:61–72.

Deguchi Y, Morimoto K. Application of an in vivo brain microdialysis technique to studies of drug transport across the blood–brain barrier. Curr Drug Metab 2001;2:411–23.

Duvvuri S, Gandhi MD, Mitra AK. Effect of P-glycoprotein on the ocular disposition of a model substrate, quinidine. Curr Eye Res 2003;27:345–53.

Engler CB, Sander B, Larsen M, Koefoed P, Parving HH, Lund-Andersen H. Probenecid inhibition of the outward transport of fluorescein across the human blood–retina barrier. Acta Ophthalmol 1994;72:663–7.

Gao B, Stieger B, Noé B, Fritschy JM, Meier PJ. Localization of the organic anion transporting polypeptide 2 (Oatp2) in capillary endothelium and choroid plexus epithelium of rat brain. J Histochem Cytochem 1999;47:1255–64.

Gao B, Wenzel A, Grimm C, Vavricka SR, Benke D, Meier PJ, et al. Localization of organic anion transport protein 2 in the apical region of rat retinal pigment epithelium. Invest Ophthalmol Vis Sci 2002;43:510–4.

Hagenbuch B, Meier PJ. The superfamily of organic anion transporting polypeptides. Biochim Biophys Acta 2003;1609:1–18.

Hosoya K, Tomi M. Advances in the cell biology of transport via the inner blood–retinal barrier: establishment of cell lines and transport functions. Biol Pharm Bull 2005;28:1–8.

Hosoya K, Tomi M, Ohtsuki S, Takanaga H, Ueda M, Yanai N, et al. Conditionally immortalized retinal capillary endothelial cell lines (TR-iBRB) expressing differentiated endothelial cell functions derived from a transgenic rat. Exp Eye Res 2001;72:163–72.

Hosoya K, Minamizono A, Katayama K, Terasaki T, Tomi M. Vitamin C transport in oxidized form across the rat blood–retinal barrier. Invest Ophthalmol Vis Sci 2004;45:1232–9.

Li JY, Boado RJ, Pardridge WM. Blood–brain barrier genomics. J Cereb Blood Flow Metab 2001;21:61–8.

Lightman SL, Palestine AG, Rapoport SI, Rechthand E. Quantitative assessment of the permeability of the rat blood–retinal barrier to small water-soluble non-electrolytes. J Physiol 1987;389:483–90.

Louzada-Junior P, Dias JJ, Santos WF, Lachat JJ, Bradford HF, Coutinho-Netto J. Glutamate release in experimental ischaemia of the retina: an approach using microdialysis. J Neurochem 1992;59:358–63.

Macha S, Mitra AK. Ocular pharmacokinetics in rabbits using a novel dual probe microdialysis technique. Exp Eye Res 2001;72:289–99.

Mikkaichi T, Suzuki T, Onogawa T, Tanemoto M, Mizutamari H, Okada M, et al. Isolation and characterization of a digoxin transporter and its rat homologue expressed in the kidney. Proc Natl Acad Sci USA 2004;101:3569–74.

Noé B, Hagenbuch B, Stieger B, Meier PJ. Isolation of a multispecific organic anion and cardiac glycoside transporter from rat brain. Proc Natl Acad Sci USA 1997;94:10346–50.

Pow DV. Amino acids and their transporters in the retina. Neurochem Int 2001;38:463–84.

Reichel C, Gao B, Van Montfoort J, Cattori V, Rahner C, Hagenbuch B, et al. Localization and function of the organic anion-transporting polypeptide Oatp2 in rat liver. Gastroenterology 1999;117:688–95.

Rittenhouse KD, Peiffer Jr RL, Pollack GM. Microdialysis evaluation of the ocular pharmacokinetics of propranolol in the conscious rabbit. Pharm Res 1999;16:736–42.

Sears ML. Pharmacology of the eye. New York: Springer-Verlag; 1983.

Sekine T, Cha SH, Endou H. The multispecific organic anion transporter (OAT) family. Pflügers Arch 2000;440:337–50.

Sen HA, Berkowitz BA, Ando N, de Juan Jr E. In vivo imaging of breakdown of the inner and outer blood–retinal barriers. Invest Ophthalmol Vis Sci 1992;33:3507–12.

Sugiyama D, Kusuhara H, Shitara Y, Abe T, Meier PJ, Sekine T, et al. Characterization of the efflux transport of 17beta-estradiol-D-17beta-glucuronide from the brain across the blood–brain barrier. J Pharmacol Exp Ther 2001;298:316–22.

Sugiyama D, Kusuhara H, Taniguchi H, Ishikawa S, Nozaki Y, Aburatani H, et al. Functional characterization of rat brain-specific organic anion transporter (Oatp14) at the blood–brain barrier: high affinity transporter for thyroxine. J Biol Chem 2003;278:43489–95.

Tomi M, Hosoya K. Application of magnetically isolated rat retinal vascular endothelial cells for the determination of transporter gene expression levels at the inner blood–retinal barrier. J Neurochem 2004;91:1244–8.

Tunblad K, Hammarlund-Udenaes M, Jonsson EN. An integrated model for the analysis of pharmacokinetic data from microdialysis experiments. Pharm Res 2004;21:1698–707.

Yamaoka K, Tanigawara Y, Nakagawa T, Uno T. A pharmacokinetic analysis program (multi) for microcomputer. J Pharmacobiodyn 1981;4:879–85.

Yano Y, Yamaoka K, Tanaka H. A nonlinear least squares program, MULTI (FILT), based on fast inverse Laplace transform for microcomputers. Chem Pharm Bull 1989;37:1035–8.

Inhibition of Dehydroascorbic Acid Transport across the Rat Blood–Retinal and –Brain Barriers in Experimental Diabetes

Akito MINAMIZONO, Masatoshi TOMI, and Ken-ichi HOSOYA*

Department of Pharmaceutics, Graduate School of Medical and Pharmaceutical Sciences, University of Toyama; 2630 Sugitani, Toyama 930–0194, Japan. Received May 19, 2006; accepted July 20, 2006; published online July 25, 2006

Vitamin C is mainly transported across the blood–retinal and –brain barriers as dehydroascorbic acid (DHA) *via* a facilitative glucose transporter, GLUT1, and accumulates as ascorbic acid in the retina and brain. To investigate whether DHA transport to the retina and brain is changed by hyperglycemia, [^{14}C]DHA transport across the blood–retinal and –brain barriers was examined using *in vivo* integration plot analysis in streptozotocin-induced diabetic rats with a 3-week duration of diabetes and in normal rats. Blood-to-retina and -brain transport of [^{14}C]DHA was reduced by 65.5% and 84.1%, respectively, in diabetic rats compared with normal rats, whereas there was no major difference in the heart. Therefore, we propose that hyperglycemia reduces the supply of vitamin C to the retina and brain.

Key words dehydroascorbic acid; GLUT1; diabetes; blood–retinal barrier; blood–brain barrier

Vitamin C plays an essential role as a cofactor involved in the enzymatic biosynthesis of collagen, catecholamine, and peptide neurohormones and antioxidant and free radical scavengers to detoxify free radicals in the retina and brain.[1] Vitamin C is present in retinal and brain tissues at high concentrations compared with other organs and there is a greater than 10-fold gradient between the concentration of ascorbic acid (AA) in the retina and brain tissues and blood.[2,3] Recent reports indicate that vitamin C is mainly transported across the blood–retinal barrier (BRB) and –brain barrier (BBB) as dehydroascorbic acid (DHA) *via* a facilitative glucose transporter, GLUT1, and accumulates as AA in the retina and brain.[4—6] DHA, which is an oxidized form of AA, is present at a concentration of 10 μM in rat and human plasma.[7,8] To maintain a high concentration of AA in the retina and brain, GLUT1 at the BRB and BBB supplies DHA to the retina and brain as well as D-glucose under normal conditions. Thus, one hypothesis to explain its action in diabetes mellitus is that hyperglycemia inhibits the supply of DHA to the retina and brain because of competitive inhibition of D-glucose for DHA transport *via* GLUT1.

The purpose of this study was to evaluate how the DHA transport to the retina and brain changes under hyperglycemic conditions by using integration plot analysis in streptozotocin-induced diabetic and normal rats.

MATERIALS AND METHODS

Animals Male Wistar rats at 3 weeks of age (body weights: 50—55 g) were purchased from SLC (Shizuoka, Japan). The investigations using rats described in this report conformed to the provisions of the Animal Care Committee, Toyama Medical and Pharmaceutical University (currently University of Toyama) (#2004-48) and the ARVO Statement on the Use of Animals in Ophthalmic and Vision Research.

Regents L-[1-^{14}C]Ascorbic acid ([^{14}C]AA, 13 mCi/mmol) was purchased from Perkin-Elmer Life Sciences (Boston, MA, U.S.A.). L-[^{14}C]Dehydroascorbic acid ([^{14}C]DHA) was generated in all experiments by incubating [^{14}C]AA (1 μM in saline) with ascorbate oxidase (1 unit/1 mmol AA in saline, Sigma, St. Louis, MO, U.S.A.) at 37 °C for 90 s as described in a previous report.[5] All other chemicals were of reagent grade and available commercially.

Animal Model of Diabetes Melitus Rats at 3 weeks of age were randomly assigned to become diabetic (n=5) or to remain non-diabetic controls (n=5). Diabetes was induced by the injection of a freshly prepared solution of streptozotocin in citrate buffer (pH 4.5) at a dose of 45 mg/kg into the tail vein, whereas non-diabetic control rats were treated with citrate buffer alone. A sample of blood was obtained from this vein over a period from 1 to 3 weeks after streptozotocin injection for measurement of the blood D-glucose concentrations to confirm the presence of hyperglycemia. Blood glucose concentrations were determined by the glucoseoxidase method (Nipro Freestyle, Osaka, Japan).

Determination of Influx Permeability Clearance The rats were anesthetized with an intramuscular injection of ketamine–xylazine (1.22 mg xylazine and 125 mg ketamine/kg) and then [^{14}C]DHA (5 μCi/rat, approximately 200 μmol DHA in 200 μl/head) was injected *via* the femoral vein. At the times designated (0.5, 1, 3 or 5 min) after administration, rats were sacrificed and the plasma and tissues were removed. Tissue sampling and determination of radioactivity were performed as described in a previous report.[5] The apparent influx permeability clearance (K_{in}) of [^{14}C]DHA in the tissue ($K_{in\ tissue}$) [μl/(min·g tissue)] was determined by integration plot analysis. As an index of the tissue distribution characteristics of [^{14}C]DHA, the apparent tissue-to-plasma concentration ratio (V_d) was used. This ratio [$V_d(t)$] (ml/g tissue) was defined as the amount of [^{14}C] per gram tissue divided by that per milliliter plasma, calculated over the time-period of the experiment. In brief, the tissue uptake rate of [^{14}C]DHA can be described by equation (Eq. 1):

$$V_d(t)=K_{in}\times AUC(t)/C_p(t)+V_i \quad (1)$$

where $C_p(t)$ (dpm/ml) and V_i (ml/g tissue) represent the plasma concentration at time t and the rapidly equilibrated distribution volume of [^{14}C]DHA, respectively; $AUC(t)$ (dpm·min/ml) is the area under the plasma concentration time curve of [^{14}C]DHA from time 0 to t. When $AUC(t)/C_p(t)$ (min) is plotted *versus* $V_d(t)$ (ml/g tissue), as shown in Fig. 1, the slope represents $K_{in\ tissue}$ [μl/(min·g tissue)].

* To whom correspondence should be addressed. e-mail: hosoyak@pha.u-toyama.ac.jp

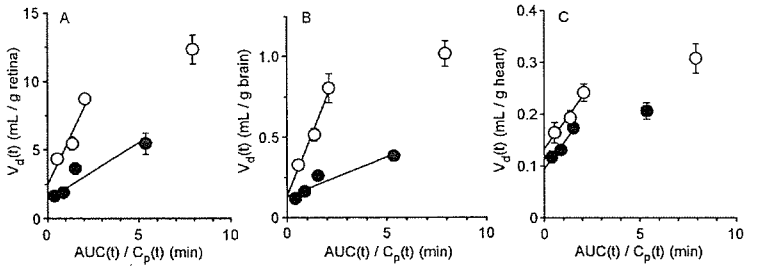

Fig. 1. Integration Plot of the Initial Uptake of [^{14}C]DHA by the Retina (A), Brain (B), and Heart (C) after Intravenous Administration

[^{14}C]DHA (5 μCi/rat) was injected into streptozotocin-induced diabetic rats (closed circle) and normal rats (open circle) *via* the femoral vein. Each point represents the mean± S.E.M. (n=3—5).

Data Analysis Unless otherwise indicated, all data represent means±S.E.M. An unpaired, two-tailed Student's t-test was used to determine the significance of differences between two group means.

RESULTS

The blood D-glucose concentration was 25.6±0.4 mM (n=5) in the streptozotocin-induced diabetic rats with a 3-week duration of diabetes, and 4.42±0.07 mM (n=10) and 8.01±0.32 mM (n=5) at 3 and 6 weeks age, respectively, in non-diabetic control rats. It was increased 3.2-fold in diabetic rats compared with controls. The final body weights were not appreciably increased in the streptozotocin-induced diabetic rats with a 3-week duration of diabetes (97.6±4.0 g, n=5), whereas the final body weights of the control rats increased to 215±5 g (n=5) from 52.0±1.0 g (n=10).

The DHA transport into the retina and brain across the BRB and BBB was evaluated and compared with the heart by means of the integration plot analysis after intravenous administration of [^{14}C]DHA to the streptozotocin-induced diabetic and normal rats (Fig. 1). The $K_{\text{in retina}}$ of [^{14}C]DHA in diabetic and normal rats was determined to be 841±243 μl/(min·g retina) and $2.44\times10^{3}\pm0.05\times10^{3}$ μl/(min·g retina), respectively. The $K_{\text{in brain}}$ of [^{14}C]DHA in diabetic and normal rats was determined to be 49.1± 11.5 μl/(min·g brain) and 309±53 μl/(min·g brain), respectively. The $K_{\text{in retina}}$ and $K_{\text{in brain}}$ of [^{14}C]DHA in diabetic rats was reduced by 65.5% and 84.1%, respectively, compared with normal rats, whereas no significant difference was found between the $K_{\text{in heart}}$ of diabetic and normal rats [50.0±12.6 μl/(min·g heart) and 49.7±15.1 μl/(min·g heart), respectively].

DISCUSSION

The present study produces, for the first time, *in vivo* evidence that hyperglycemia reduces blood-to-retina and -brain transport of [^{14}C]DHA across the BRB and BBB (Fig. 1). DHA is transported by GLUT1, which is expressed at the luminal (blood) and abluminal (retina or brain) side of the inner BRB (retinal capillary endothelial cells), outer BRB (retinal pigment epithelial cells), and BBB (brain capillary endothelial cells).[9—11] On the other hand, there was only a small difference between the $K_{\text{in heart}}$ of diabetic and normal rats since there is no barrier in the heart. Therefore, DHA transport from blood to the retina and brain decreases with increasing blood D-glucose concentration because of prevention of DHA uptake by GLUT1 at the BRB and BBB. We previously reported that [^{14}C]DHA uptake by a retinal endothelial cell line (TR-iBRB2 cells) expressing GLUT1 was inhibited by D-glucose in a concentration-dependent manner with a 50% inhibition of 5.56 mM.[5] Although DHA transport *via* GLUT1 at the BRB and BBB is not completely inhibited under normal conditions, it is markedly inhibited under diabetic conditions. Indeed, the $K_{\text{in retina}}$ and $K_{\text{in brain}}$ of [^{14}C]DHA in diabetic rats was reduced by 65.5% and 84.1%, respectively, compared with normal rats (Fig. 1). Badr *et al.* reported that streptozotocin-induced diabetic rats with a 8-week duration of diabetes exhibited reduced GLUT1 expression by >60% at the inner BRB compared with non-diabetic rats, but this resulted in no reduction in GLUT1 expression at the outer BRB and BBB.[12] On the other hand, Pardridge *et al.* reported that streptozotocin-induced diabetic rats with a 1-week duration of diabetes exhibited reduced GLUT1 expression by 77% at the BBB compared with non-diabetic rats.[13] Although down-regulation of GLUT1 expression is not constant under different experimental conditions, reduction of GLUT1 expression at the BRB and BBB cannot be ruled out as a contributor to DHA transport to the retina and brain in the present study. When the GLUT1 expression at the BBB was reduced by 77%, the GLUT1 transport activity at the BBB was only reduced by 44%.[13] Therefore, hyperglycemia plays a role in reducing the supply of DHA to the brain and retina even although GLUT1 is down-regulated.

Since there is no compensatory down-regulation of GLUT1 at the inner BRB in an animal model and in patients with long-standing diabetes,[14,15] reduction of DHA transport by hyperglycemia is more involved in the chronic hyperglycemia of long-standing diabetes than acute hyperglycemia. The total vitamin C concentration in the retina and brain is not changed in short-term diabetics, since AA/DHA could be recycled by glutathione.[16,17] However, the chronic hyperglycemia of long-standing diabetes is associated with "glucose toxicity" leading to oxidative stress resulting from increased production of reactive oxygen species and, often, down-regulation of anti-oxidative defense mechanisms.[18,19] Hyperglycemia reduces DHA transport *via* GLUT1 at the BRB and BBB. DHA is reconverted into AA in the retina and brain.[4,5] Reduction of the supply of AA to the retina and brain through competition of D-glucose and DHA for a common transporter would reduce the antioxidant and could lead to accumulation of reactive oxygen species followed by acti-

vation of the protein kinase C and aldose reductase pathway and advanced glycation end-products in the retina and brain.[20] Moreover, AA is a required cofactor for several intracellular hydroxylases, including proline hydroxylase and dopamine-β-hydroxylase.[1] Therefore, chronic hyperglycemia appears to cause disregulation of catecholamine metabolism in the retina and brain. In the light of these findings, diabetic patients may experience enhanced oxidative stress and metabolic perturbations in the retina and brain by reducing the influx transport of DHA, leading to the hypothesis that diabetic retinopathy and encephalopathy involve a dysfunction of DHA influx transport at the BRB and BBB.

In conclusion, hyperglycemia reduces blood-to-retina and -brain transport of DHA across the BRB and BBB. These findings provide important information to help us understand the implications of increasing the antioxidant potential in the retina and brain.

Acknowledgements The authors would like to thank Drs. Kazunori Katayama and Ikuko Kimura for valuable discussions. This study was supported, in part, by a Grant-in-Aid for Scientific Research from the Japan Society for the Promotion of Science and a grant for Research on Sensory and Communicative Disorders by the Ministry of Health, Labor, and Welfare, Japan.

REFERENCES

1) Friedman P. A., Zeidel M. L., *Nature Med.*, **5**, 620—621 (1999).
2) Kaufman S., *Phamacol. Rev.*, **18**, 61—69 (1966).
3) Nielsen J. C., Naash M. I., Anderson R. E., *Invest. Ophthalmol. Vis. Sci.*, **29**, 22—26 (1987).
4) Agus D. B., Gambhir S. S., Pardridge W. M., Spielholz C., Baselga J., Vera J. C., Golde D. W., *J. Clin. Invest.*, **100**, 2842—2848 (1997).
5) Hosoya K., Minamizono A., Katayama K., Terasaki T., Tomi M., *Invest. Ophthalmol. Vis. Sci.*, **45**, 1232—1239 (2004).
6) Tomi M., Hosoya K., *J. Neurochem.*, **91**, 1244—1248 (2004).
7) Koshiishi I., Imanari T., *J. Chromatogr. B*, **709**, 150—156 (1998).
8) Nakayama H., Akiyama S., Inagaki M., Gotoh Y., Oguchi K., *Nephrol. Dial. Transplant.*, **16**, 574—579 (2001).
9) Pardridge W. M., Boado R. J., Farrell C. R., *J. Biol. Chem.*, **265**, 18035—18040 (1990).
10) Takata K., Kasahara T., Kasahara M., Ezaki O., Hirano H., *Invest. Ophthalmol. Vis. Sci.*, **33**, 377—383 (1992).
11) Kumagai A. K., Glasgow B. J., Pardridge W. M., *Invest. Ophthalmol. Vis. Sci.*, **35**, 2887—2894 (1994).
12) Badr G. A., Tang J., Ismail-Beigi F., Kern T. S., *Diabetes*, **49**, 1016—1021 (2000).
13) Pardridge W. M., Triguero D., Farrell C. R., *Diabetes*, **39**, 1040—1044 (1990).
14) Kumagai A. K., Vinorces S. A., Pardridge W. M., *Brain Res.*, **706**, 313—317 (1996).
15) Fernandes R., Suzuki K., Kumagai A. K., *Invest. Ophthalmol. Vis. Sci.*, **44**, 3150—3154 (2003).
16) May J. M., Qu Z., Li X., *Biochem. Pharmacol.*, **62**, 873—881 (2001).
17) Obrosova I. G., Minchenko A. G., Marinescu V., Fathallah L., Kennedy A., Stockert C. M., Frank R. N., Stevens M. J., *Diabetologia*, **44**, 1102—1110 (2001).
18) Lorenzi M., Gerhardinger C., *Diabetologia*, **44**, 791—804 (2001).
19) Mastrocola R., Restivo F., Vercellinatto I., Danni O., Brignardello E., Aragno M., Boccuzzi G., *J. Endocrinol.*, **187**, 37—44 (2005).
20) Root-Bernstein R., Busik J. V., Henry D. N., *J. Theor. Biol.*, **216**, 345—359 (2002).

0013-7227/06/$15.00/0
Printed in U.S.A.

Endocrinology 147(2):1020–1028

doi: 10.1210/en.2005-0825

Altered Subcellular Distribution of Estrogen Receptor α Is Implicated in Estradiol-Induced Dual Regulation of Insulin Signaling in 3T3-L1 Adipocytes

Kiyofumi Nagira, Toshiyasu Sasaoka, Tsutomu Wada, Kazuhito Fukui, Mariko Ikubo, Satoko Hori, Hiroshi Tsuneki, Shigeru Saito, and Masashi Kobayashi

Departments of Obstetrics and Gynecology (K.N., S.S.) and Clinical Pharmacology (T.W., S.H., H.T., T.S.) and First Department of Medicine (K.F., M.I., M.K.), University of Toyama, 2630 Sugitani, Toyama 930-0194, Japan

We investigated the mechanisms by which estrogen alters insulin signaling in 3T3-L1 adipocytes. Treatment with 17β-estradiol (E2) did not affect insulin-induced tyrosine phosphorylation of insulin receptor. E2 enhanced insulin-induced tyrosine phosphorylation of insulin receptor substrate-1 (IRS-1), IRS-1/p85 association, phosphorylation of Akt, and 2-deoxyglucose uptake at 10^{-8} M, but inhibited these effects at 10^{-5} M. A concentration of 10^{-5} M E2 enhanced insulin-induced phosphorylation of IRS-1 at Ser^{307}, which was abolished by treatment with a c-Jun NH_2-terminal kinase inhibitor. In addition, the effect of E2 was abrogated by pretreatment with a specific estrogen receptor antagonist, ICI182,780. Membrane-impermeable E2, E2-BSA, did not affect the insulin-induced phosphorylation of Akt at 10^{-8} M, but inhibited it at 10^{-5} M. Furthermore, E2 decreased the amount of estrogen receptor α at the plasma membrane at 10^{-8} M, but increased it at 10^{-5} M. In contrast, the subcellular distribution of estrogen receptor β was not altered by the treatment. These results indicate that E2 affects the metabolic action of insulin in a concentration-specific manner, that high concentrations of E2 inhibit insulin signaling by modulating phosphorylation of IRS-1 at Ser^{307} via a c-Jun NH_2-terminal kinase-dependent pathway, and that the subcellular redistribution of estrogen receptor α in response to E2 may explain the dual effect of E2. (*Endocrinology* 147: 1020–1028, 2006)

HUMAN PREGNANCY IS associated with hyperinsulinemia and a progressive decline in insulin sensitivity (1). Thus, a number of clinical studies indicate that insulin resistance occurs in late pregnancy (2, 3). The cellular changes in insulin resistance during late pregnancy have been ascribed to altered levels of placental-derived hormones, including estrogen, progesterone, and human placental lactogen (4). Among these sex steroids, high concentrations of estrogen are known to inhibit insulin-stimulated glucose uptake in cultured cells (5). In addition, increased levels of TNF-α have been associated with insulin resistance in late pregnancy (6). Thus, estrogen and TNF-α produced in the placenta appear to play a key role in insulin resistance (5, 6). Although the mechanism of insulin resistance caused by TNF-α has been studied intensively, the mechanism by which estrogen induces insulin resistance is unknown (6). In contrast, physiological levels of estrogen are known to protect against insulin resistance in women (7). Along this line, clinical studies suggest that after menopause women have an increased risk of developing diabetes (8, 9). Therefore, estrogen appears to control glucose homeostasis in a concentration-specific manner. The insulin signaling system leading to glucose uptake has been studied intensively in 3T3-L1 adipocytes (10).

The binding of insulin to the α-subunit of the insulin receptor results in autophosphorylation and activation of the β-subunit (11–13). The activated insulin receptor phosphorylates insulin receptor substrate-1 (IRS-1) at tyrosine residues (11–13). Tyrosine-phosphorylated IRS-1 binds to the p85 subunit of phosphatidylinositol 3-kinase (PI3-kinase), leading to the activation of the p110 catalytic subunit (11–13). PI3-kinase generates PI triphosphate from PI-bisphosphate, leading to the phosphorylation and activation of Akt (11–13). Akt is known to be an important mediator of the insulin-induced uptake of glucose (14). The cellular mechanisms by which estrogen affects the insulin signaling system are unknown.

Estrogen binds receptors of two subtypes: estrogen receptor α, first identified in 1986, and estrogen receptor β, cloned subsequently (15, 16). Estrogen receptors are expressed not only in the reproductive organs of males and females, but also in nonreproductive tissues, including fat tissues (17, 18). It has been shown that the effect of estrogen is mediated by the binding of estrogen receptors in the cytosol, resulting in translocation and transcriptional activation in the nucleus (19). In addition, recent reports suggest a nontranscriptional action mediated by the estrogen receptor (20). Along these lines, estrogen receptors are distributed in the plasma membrane in addition to the cytosol and nucleus (21). However, the role of estrogen receptors at specific cellular locations in the regulation of insulin signaling is unknown.

In the present study we studied the effect of the main estrogen, estradiol (E2), on insulin signaling leading to glucose uptake in 3T3-L1 adipocytes. In addition, to clarify the

First Published Online November 3, 2005

Abbreviations: 2-DOG, 2-Deoxyglucose; CS-, charcoal-stripped; E2, 17β-estradiol, estradiol; FBS, fetal bovine serum; HES, HEPES sucrose; IRS-1, insulin receptor substrate-1; JNK, c-Jun NH_2-terminal kinase; PI, phosphatidylinositol 3-kinase; PMSF, phenylmethylsulfonylfluoride.

Endocrinology is published monthly by The Endocrine Society (http://www.endo-society.org), the foremost professional society serving the endocrine community.

molecular mechanism by which E2 affects the insulin signaling system, we investigated the isoform and subcellular distribution of the estrogen receptor mediating the effect of E2.

Materials and Methods

Materials

Recombinant human insulin was provided by Lilly Research Laboratories (Indianapolis, IN). Recombinant human TNF-α was supplied by Dainippon Pharmaceutical Co. (Osaka, Japan). 17β-Estradiol (E2) and E2-BSA were purchased from Sigma-Aldrich Corp. (St. Louis, MO). A complete estrogen receptor antagonist, ICI182,780, was obtained from Tocris (Ellisville, MO). The Jun NH_2-terminal kinase (JNK) inhibitor, SP600125, was purchased from BIOMOL (Plymouth Meeting, PA). 2-[1,2-^{3}H]Deoxyglucose (2-DOG) was obtained from DuPont NEN Life Science Products (Boston, MA). A monoclonal antiphosphotyrosine antibody (PY20) was purchased from Transduction Laboratories (Lexington, KY). A polyclonal anti-IRS-1 antibody, a polyclonal anti-Ser^{307} phosphospecific IRS-1 antibody, a polyclonal anti-Ser^{612} phosphospecific IRS-1 antibody, a polyclonal anti-Ser^{636} phosphospecific IRS-1 antibody, a monoclonal anti-p85 antibody, a polyclonal anti-Ser^{473} phosphospecific Akt antibody, a polyclonal anti-Thr^{308} phosphospecific Akt antibody, and a polyclonal anti-Akt antibody were obtained from Upstate Biotechnology, Inc. (Lake Placid, NY). A polyclonal antiinsulin receptor antibody, horseradish peroxidase-conjugated antimouse and antirabbit IgG antibodies, a polyclonal antiestrogen receptor α antibody, and a polyclonal antiestrogen receptor β antibody were purchased from Santa Cruz Biotechnology, Inc. (Santa Cruz, CA). Phenol red-free DMEM and fetal bovine serum (FBS) were obtained from Invitrogen Life Technologies, Inc. (Gaithersburg, MD). Protein G-Sepharose was purchased from Pharmacia Biotech (Uppsala, Sweden). Reagents for electrophoresis were obtained from Bio-Rad Laboratories, Inc. (Hercules, CA). All other reagents were of analytical grade and purchased from Sigma-Aldrich Corp. or Wako Pure Chemical Industries (Osaka, Japan).

Cell culture and treatment

3T3-L1 fibroblasts were grown and passaged in phenol red-free DMEM supplemented with 10% donor calf serum. Cells, 2 d after confluence, were used for differentiation. The differentiation medium contained 10% charcoal-stripped FBS (CS-FBS), 0.5 mM 3-isobutyl-1-methylxanthine, 1 μM dexamethasone, and 1 μM insulin. After charcoal stripping, E2 and estrone concentrations in serum decreased from 0.48 to less than 0.07 pM and from 0.36 to less than 0.12 pM, respectively. After 3 d, the differentiation medium was replaced with postdifferentiation medium containing 10% CS-FBS and 800 nM insulin. After 3 more days, the postdifferentiation medium was replaced with phenol red-free DMEM supplemented with 10% CS-FBS. The medium was changed every 3 d until the cells were used for experiments. Fourteen to 16 d after the induction of differentiation, more than 95% of the cells had morphological and biochemical properties of adipocytes. E2 dissolved in ethanol and TNF-α in PBS were added to the cell culture medium, in which 10^6 cells were contained/plate, without FBS for 16 h.

2-DOG uptake

3T3-L1 adipocytes derived from differentiation of 3T3-L1 fibroblasts were grown in six-well multiplates and were serum-starved for 3 h. The cells were stimulated with 17 nM insulin for 15 min in Krebs-Ringer-phosphate-HEPES buffer containing 10 mM HEPES, 131.2 mM NaCl, 4.7 mM KCl, 1.2 mM $MgSO_4$, 2.5 mM $CaCl_2$, and 2.5 mM NaH_2PO_4, and 1% BSA (pH 7.4). 2-[^{3}H]DOG (0.1 mM; 0.4 kBq/well) was added for 4 min. The reaction was stopped by the addition of 10 μM cytochalasin B. The cells were washed three times with ice-cold PBS and solubilized with 0.2% sodium dodecyl sulfate-0.2 N NaOH (22, 23). The radioactivity incorporated into the cells was measured by liquid scintillation counting. The results were corrected for nonspecific uptake determined by 2-[^{3}H]DOG uptake in the presence of 10 μM cytochalasin B. Nonspecific binding was less than 10% of the total uptake.

Subcellular fractionation

The cells were washed twice with PBS and once with HEPES sucrose (HES) buffer containing 255 mM sucrose, 20 mM HEPES, 1 mM EDTA, 1 mM phenylmethylsulfonylfluoride (PMSF), 1 mM Na_3VO_4, 2 μg/ml aprotinin, and 50 ng/ml okadaic acid (pH 7.4). The cells were then immediately homogenized by 20 strokes with a motor-driven homogenizer in HES buffer containing 20 mM HEPES, 255 mM sucrose, 1 mM EDTA, 1 mM PMSF, 1 mM Na_3VO_4, 2 μg/ml aprotinin, and 50 ng/ml okadaic acid (pH 7.4) at 4 C. The homogenates obtained from two 10-cm diameter dishes per condition were subjected to subcellular fractionation to isolate the plasma membrane, cytosol, and nucleus as described previously (24). In brief, the homogenates were centrifuged at 19,000 $\times$ *g* for 20 min. The resulting supernatant was centrifuged at 250,000 $\times$ *g* for 90 min. The remaining supernatant was centrifuged at Centricon-30 (Amicon, Inc., Beverly, MA) and used as cytosol. The pellet obtained from the initial spin was resuspended in HES buffer, layered onto a 1.12-M sucrose cushion, and centrifuged at 100,000 $\times$ *g* in a swing rotor for 60 min. A white fluffy band at the interface was collected, resuspended in HES buffer, and centrifuged at 40,000 $\times$ *g* for 20 min, yielding a pellet of plasma membrane. A viscous brown pellet was collected, yielding a pellet of nucleus. The purities of the nuclear and cytosolic preparations were determined by examining histone as a nuclear marker and calpain as a cytosolic marker. The samples were adjusted to a final protein concentration of 1–3 mg/ml, which was measured by the Bradford method, and stored at −80 C before use.

Immunoprecipitation and Western blotting

The cells or cell preparations were lysed in a buffer containing 30 mM Tris, 150 mM NaCl, 10 mM EDTA, 1% Nonidet P-40, 1 mM PMSF, 1 mM Na_3VO_4, 50 nM sodium fluoride, 10 μg/ml aprotinin, and 1 μM leupeptin (pH 7.4) for 30 min at 4 C. The lysates were centrifuged to remove insoluble materials. The supernatants (100 μg protein) were immunoprecipitated with antibodies for 16 h at 4 C. The immunoprecipitates or total cell lysates were then separated by 7.5% or 15% SDS-PAGE and transferred onto polyvinylidene difluoride membranes (Millipore Corp., Bedford, MA) using a Bio-Rad Transblot apparatus. The membranes were blocked in a buffer containing 50 mM Tris, 150 mM NaCl, 0.1% Tween 20, and 2.5% BSA or 5% nonfat milk (pH 7.5) for 2 h at 20 C. They were then probed with antibodies for 2 h at 20 C or for 16 h at 4 C. After the membranes had been washed in a buffer containing 50 mM Tris, 150 mM NaCl, and 0.1% Tween 20 (pH 7.5), blots were incubated with a horseradish peroxidase-linked secondary antibody and subjected to enhanced chemiluminescence detection using ECL reagent according to the manufacturer's instruction (Amersham Biosciences, Indianapolis, IN) (25, 26). In each experiment, the intensity of the band derived from control cells was averaged and assigned a value of 1 arbitrary unit, and the intensities of all treated groups were expressed relative to this value.

Statistical analysis

Experiments were separately conducted at least four times, and data are presented as the mean ± SE. *P* values were determined by ANOVA and Scheffé test. $P < 0.05$ was considered statistically significant.

Results

Effect of E2 on insulin-stimulated glucose uptake

We first examined the concentration-dependent effect of E2 on insulin-stimulated 2-DOG uptake in 3T3-L1 adipocytes (Fig. 1A). Insulin at 17 nM stimulated 2-DOG uptake by 6.5 ± 0.6-fold in 3T3-L1 adipocytes. Low concentrations of E2 further increased uptake. Insulin-induced 2-DOG uptake was increased 18.3 ± 3.6% by treatment with 10^{-8} M E2 compared with that without E2 treatment. Conversely, concentrations of E2 above 10^{-7} M inhibited insulin-stimulated 2-DOG uptake. After treatment with 10^{-5} M E2, insulin-induced 2-DOG uptake was decreased by 25.8 ± 3.7% compared with that without E2 treatment. Insulin stimulated 2-DOG uptake in a

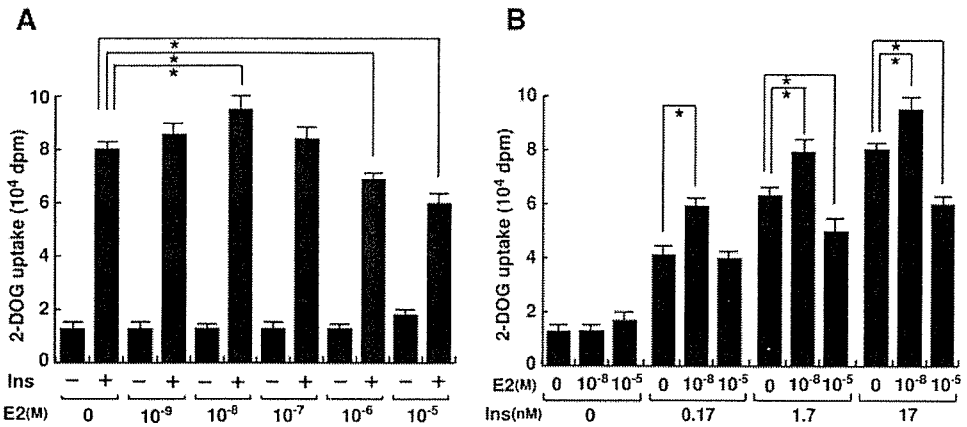

FIG. 1. Effect of E2 on insulin-induced 2-DOG uptake in 3T3-L1 adipocytes. A, Serum-starved cells treated with various concentrations of E2 for 16 h were then stimulated with 17 nM insulin for 15 min. B, Serum-starved cells treated with vehicle in ethanol, 10^{-8} M E2, or 10^{-5} M E2 were stimulated with various concentrations of insulin. Then the uptake of 2-[^{3}H]DOG for 4 min was studied. Each measurement was performed in duplicate, and results are the mean ± SE of seven separate experiments. *, $P < 0.05$ *vs.* 2-DOG uptake in control cells at the respective concentration of insulin without E2, by ANOVA and Scheffé's test.

concentration-dependent manner (Fig. 1B). Treatment with 10^{-8} M E2 significantly enhanced 0.17, 1.7, and 17 nM insulin-induced 2-DOG uptake, whereas 10^{-5} M E2 apparently inhibited 1.7 and 17 nM insulin-stimulated glucose uptake. E2 treatment alone for up to 16 h did not stimulate glucose uptake, and the amount of glucose transporter 4 was not altered by treatment with any concentration of E2 (data not shown).

Effect of E2 on early steps of insulin signaling

Because E2 affected insulin-stimulated glucose uptake, the possible involvement of E2 in the early steps of insulin signaling was examined. Insulin-induced tyrosine phosphorylation of the insulin receptor was not affected by treatment with E2 at any concentration (Fig. 2A). Interestingly, insulin-induced tyrosine phosphorylation of IRS-1 and the associa-

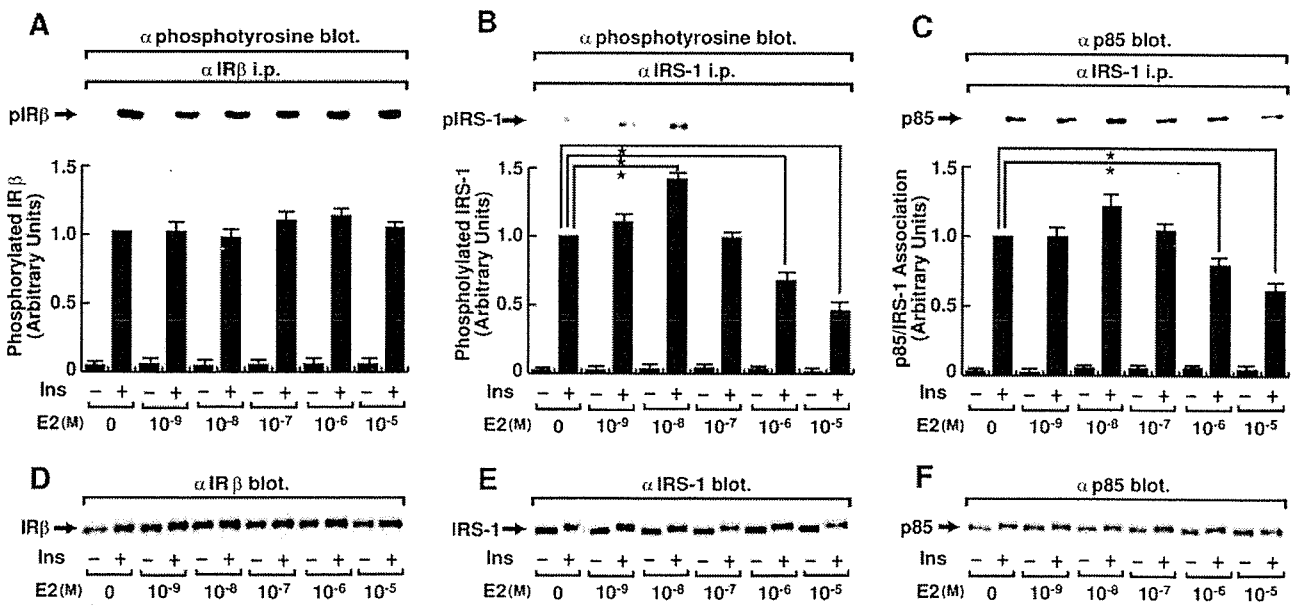

FIG. 2. Effect of E2 on early steps of insulin signaling. Serum-starved cells treated with various concentrations of E2 were stimulated with 17 nM insulin for 5 min. A, The cell lysates were immunoprecipitated with antiinsulin receptor antibody, and the precipitates were immunoblotted with antiphosphotyrosine antibody. B, The cell lysates were immunoprecipitated with anti-IRS-1 antibody, and the precipitates were immunoblotted with antiphosphotyrosine antibody. C, The cell lysates were immunoprecipitated with anti-IRS-1 antibody, and the precipitates were immunoblotted with anti-p85 antibody. Results are the mean ± SE of six separate experiments. *, $P < 0.05$ *vs.* insulin-induced phosphorylation of insulin receptor, phosphorylation of IRS-1, or association of p85 with IRS-1 in control cells stimulated with insulin in the absence of E2, by ANOVA and Scheffé's test. Total cell lysates were immunoblotted with antiinsulin receptor antibody (D), anti-IRS-1 antibody (E), or anti-p85 antibody (F).

tion of IRS-1 with the p85 subunit of PI3-kinase were promoted by treatment with a physiological concentration of E2. Thus, insulin-stimulated tyrosine phosphorylation of IRS-1 and IRS-1/p85 association were increased by 41.7 ± 3.4% and 22.9 ± 5.9%, respectively, after treatment with 10^{-8} M E2. In contrast, they were inhibited by treatment with concentrations of E2 above 10^{-7} M. At 10^{-5} M, E2 inhibited the insulin-induced tyrosine phosphorylation of IRS-1 and IRS-1/p85 association by 53.7 ± 3.7% and 25.9 ± 3.4%, respectively (Fig. 2, B and C). Amounts of protein among samples were confirmed to be equal by immunoblotting with antiinsulin receptor antibody (Fig. 2D), anti-IRS-1 antibody (Fig. 2E), and anti-p85 antibody (Fig. 2F).

Effect of E2 on insulin-induced phosphorylation of Akt

Akt lies downstream of PI3-kinase and is important for insulin's stimulation of glucose uptake (23, 27, 28). Because Akt is activated by phosphorylation at Ser^{473} and Thr^{308}, we examined the effect of E2 on the insulin-induced phosphorylation of Akt (Fig. 3, A and B). Consistent with the results of insulin-induced tyrosine phosphorylation of IRS-1 and IRS-1/p85 association, insulin-induced phosphorylation of Akt was increased by treatment with low concentrations of E2 and decreased by treatment with high concentrations of E2. Insulin-induced phosphorylation of Akt at Ser^{473} and Thr^{308} was enhanced 22.0 ± 3.3% and 30.1 ± 3.2%, respectively, by treatment with 10^{-8} M E2, whereas it was inhibited 44.7 ± 3.5% and 50.8 ± 3.6%, respectively, by treatment with 10^{-5} M E2. Amounts of protein among samples were confirmed to be equal by immunoblotting with anti-Akt antibody (Fig. 3C).

Effect of combined presence of E2 and TNF-α on insulin-stimulated tyrosine phosphorylation of IRS-1 and serine phosphorylation of Akt

TNF-α together with estrogen are secreted from the placenta and are known to be involved in insulin resistance in the late phases of pregnancy, especially in preeclampsia (29, 30). The effect of combined presence of E2 (10^{-6} M) and TNF-α on the insulin-induced tyrosine phosphorylation of IRS-1 and serine phosphorylation of Akt was examined. Insulin-induced tyrosine phosphorylation of IRS-1 was inhibited 24.6 ± 2.9% and 35.7 ± 3.6% by treatment with E2 and TNF-α, respectively (Fig. 4A). Insulin signaling was maximally inhibited by treatment with 50 ng/ml TNF-α. Treatment with both E2 and TNF-α further inhibited insulin signaling by 61.3 ± 4.2%. Similarly, treatment with E2, TNF-α, or both inhibited the insulin-induced phosphorylation of Akt by 21.8 ± 3.3%, 34.9 ± 3.0%, and 65.4 ± 3.3%, respectively (Fig. 4B). These results indicate that TNF-α combined with a submaximal concentration of E2 further inhibit insulin signaling, leading to glucose uptake.

Effect of E2 on insulin-induced serine phosphorylation of IRS-1

E2 affected insulin signaling at least at the level of tyrosine phosphorylation of IRS-1. Because tyrosine phosphorylation of IRS-1 is modulated by serine phosphorylation of IRS-1

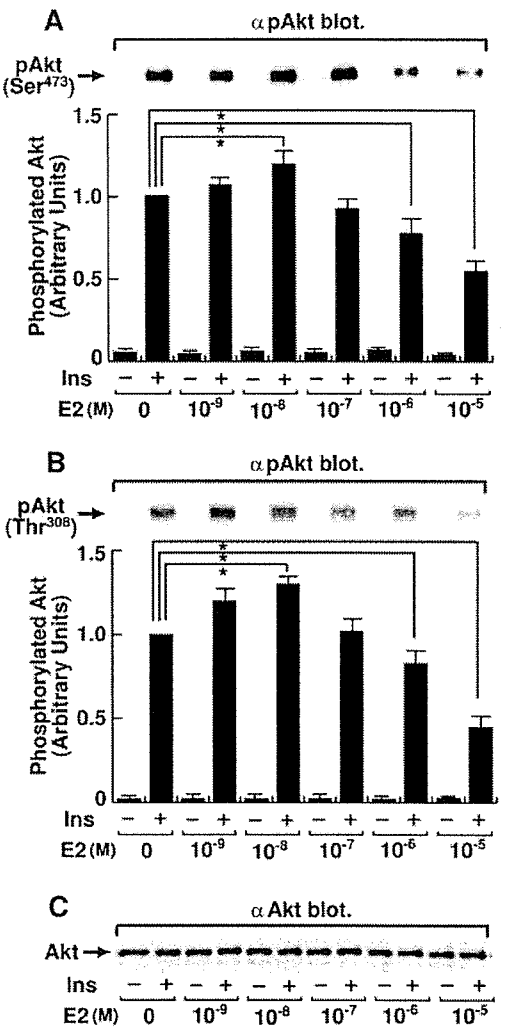

FIG. 3. Effect of E2 on insulin-induced phosphorylation of Akt. Serum-starved cells treated with various concentrations of E2 were stimulated with 17 nM insulin for 5 min. The cell lysates were immunoblotted with antiphospho-Ser^{473}-specific Akt antibody (A), antiphospho-Thr^{308}-specific Akt antibody (B), or anti-Akt antibody (C). Results are the mean ± SE of four separate experiments. *, $P < 0.05$ *vs.* insulin-induced phosphorylation of Akt without E2 treatment, by ANOVA and Scheffé's test.

(31), we examined the effect of E2 on the insulin-induced serine phosphorylation of IRS-1 (Fig. 5). The insulin-induced phosphorylation of IRS-1 at Ser^{307} was increased by treatment with E2 in a concentration-dependent manner. The extent of phosphorylation at Ser^{307} was increased 73.9 ± 4.1% by treatment with 10^{-5} M E2 (Fig. 5A). In contrast, the insulin-induced phosphorylation of IRS-1 at Ser^{612} (Fig. 5B) and Ser^{636} (Fig. 5C) was not altered by treatment with E2. These results indicate that a high concentration of E2 inhibits insulin signaling at the level of IRS-1 at least in part by increasing the phosphorylation of IRS-1 at Ser^{307}.

Effect of a JNK inhibitor on the alteration of insulin signaling caused by E2 treatment

Because IRS-1 is known to be phosphorylated by JNK at Ser^{307} (32), we examined the influence of a JNK inhibitor,

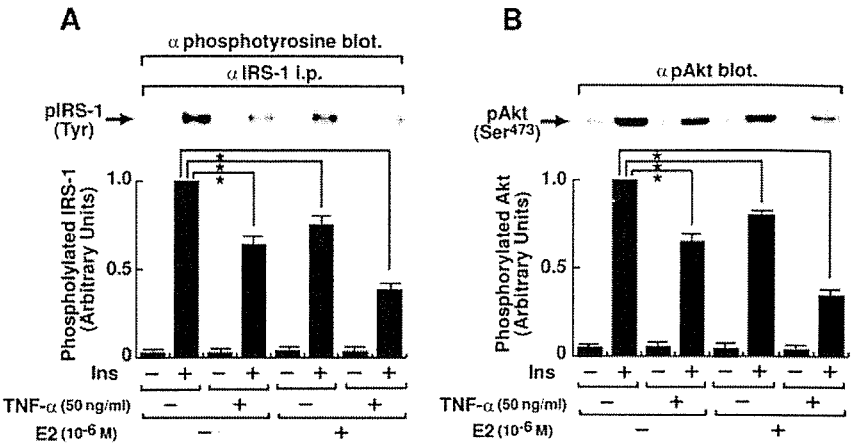

FIG. 4. Effect of the combined presence of E2 and TNF-α on insulin signaling. Serum-starved cells treated with 10^{-6} M E2 and/or 50 ng/ml TNF-α were stimulated with 17 nM insulin for 5 min. A, The cell lysates were immunoprecipitated with anti-IRS-1 antibody. The precipitates were immunoblotted with antiphosphotyrosine antibody. B, Total cell lysates were immunoblotted with antiphospho-Ser^{473}-specific Akt antibody. Results are the mean ± SE of four separate experiments. *, $P < 0.05$ *vs.* insulin-induced phosphorylation of IRS-1 and Akt without E2 and TNF-α treatment, by ANOVA and Scheffé's test.

SP600125, on the effect of E2. The enhancement of the insulin-induced phosphorylation at Ser^{307} caused by 10^{-5} M E2 was abrogated by treatment with the JNK inhibitor (Fig. 6A). As a result, inhibition of the insulin-induced tyrosine phosphorylation of IRS-1 (Fig. 6B) and serine phosphorylation of Akt (Fig. 6C) caused by E2 treatment was restored by pretreatment with the JNK inhibitor.

Effects of ICI182,780 and E2-BSA on E2-induced alteration of insulin signaling

We employed a specific estrogen receptor antagonist, ICI182,780, to examine whether the stimulatory effect of E2 on insulin signaling seen at 10^{-8} M is mediated by estrogen receptor (Fig. 7A). Pretreatment with 10 μM ICI 182,780 abrogated the enhancement of insulin-induced tyrosine phosphorylation of IRS-1 (data not shown) and serine phosphorylation of Akt caused by 10^{-8} M E2. Pretreatment with 1 μM ICI182,780 had the same effect. Similarly, we examined the effect of ICI182,780 to clarify whether the inhibitory effect of E2 at 10^{-5} M on insulin signaling is mediated by the estrogen receptor. Pretreatment with ICI182,780 at 10 μM, but not at 1 μM, restored the inhibition of insulin-stimulated tyrosine phosphorylation of IRS-1 (data not shown) and serine phosphorylation of Akt caused by 10^{-5} M E2. These results indicate that the estrogen receptor is implicated in the effects of both concentrations of E2 on insulin signaling.

The estrogen receptor is located on the plasma membrane in addition to the cytosol and nucleus (21). To examine the impact of membrane-based estrogen receptors, a membrane-impermeable E2, E2-BSA, was employed. Insulin-induced tyrosine phosphorylation of IRS-1 (data not shown) and serine phosphorylation of Akt were not enhanced by 10^{-8} M E2-BSA in contrast to E2 (Fig. 7B). However, higher concentrations of E2-BSA inhibited these actions, similar to the results obtained with E2. Thus, 10^{-5} M E2-BSA inhibited the insulin-induced tyrosine phosphorylation of IRS-1 and serine phosphorylation of Akt by 54.9 ± 3.5% (data not shown) and 49.4 ± 4.1%, respectively (Fig. 7B). These results indicate that estrogen receptors at the plasma membrane are implicated in the inhibitory effect of E2 at high concentrations, but are not involved in the enhancing effect of E2 at low concentrations.

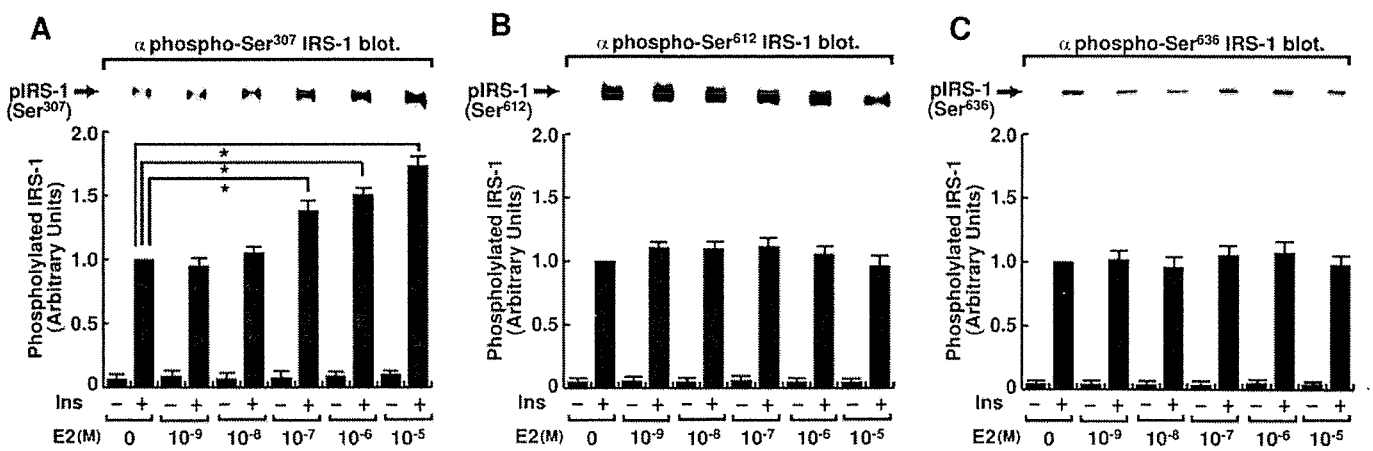

FIG. 5. Effect of E2 on insulin-induced serine phosphorylation of IRS-1. Serum-starved cells treated with various concentrations of E2 were stimulated with 17 nM insulin for 10 min. The cell lysates were immunoprecipitated with anti-IRS-1 antibody. The precipitates were immunoblotted with antiphospho-Ser^{307}-specific IRS-1 antibody (A), antiphospho-Ser^{612}-specific IRS-1 antibody (B), or antiphospho-Ser^{636}-specific IRS-1 antibody (C). Results are the mean ± SE of four separate experiments. *, $P < 0.05$ *vs.* insulin-induced serine phosphorylation of IRS-1 without E2 treatment, by ANOVA and Scheffé's test.

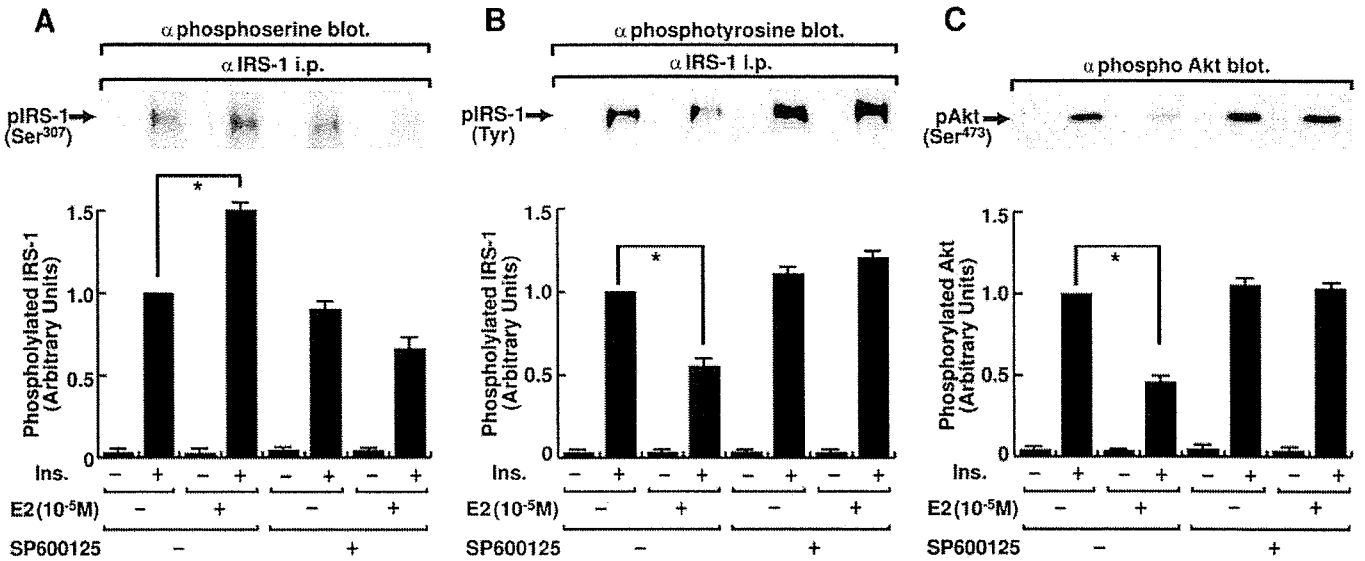

FIG. 6. Effect of a JNK inhibitor on the alteration of insulin signaling caused by E2. Serum-starved cells treated with 10^{-5} M E2 and 20 μM of the JNK inhibitor SP600125 for 16 h were stimulated with 17 nM insulin for 10 min. The cell lysates were immunoprecipitated with anti-IRS-1 antibody. The precipitates were immunoblotted with antiphospho-Ser^{307}-specific IRS-1 antibody (A) or antiphosphotyrosine antibody (B). Whole-cell lysates were immunoblotted with antiphospho-Ser^{473}-specific Akt antibody (C). Results are the mean ± SE of four separate experiments. *, $P < 0.05$ *vs.* insulin-induced serine phosphorylation of IRS-1, tyrosine phosphorylation of IRS-1, or serine phosphorylation of Akt without E2 and SP600125 treatment, by ANOVA and Scheffé's test.

Effect of E2 treatment on subcellular distribution of estrogen receptors α and β

We also investigated the subcellular redistribution of the estrogen receptor in response to E2. Treatment with 10^{-8} M E2 reduced the amount of estrogen receptor α at the plasma membrane by 17.1 ± 2.9%, but increased the amount in the nucleus by 90.7 ± 4.4%. The amount of estrogen receptor α in the cytosol was not apparently changed by E2 treatment. In contrast, treatment with 10^{-5} M E2 increased the amount of estrogen receptor α at the plasma membrane by 71.3 ± 4.1%, but decreased it in the cytosol and nucleus by 36.3 ± 3.8% and 47.3 ± 3.4%, respectively (Fig. 8, A–C). In contrast, the amounts of estrogen receptor β at the plasma membrane, in the cytosol, and in the nucleus were not apparently altered by treatment with any concentration of E2 (Fig. 8, D–F). In addition, insulin treatment did not appear to alter the subcellular distribution of estrogen receptors.

Discussion

Our results demonstrated that treatment with a physiological concentration of E2 (10^{-8} M) enhanced the insulin-induced uptake of glucose, whereas treatment with a high concentration of E2 (10^{-5} M) inhibited it. These results clearly indicate that E2 controls glucose metabolism in a concentration-specific manner. These results are consistent with clinical reports that the incidence of type 2 diabetes increases in women after menopause, and that insulin resistance occurs in women during late pregnancy (4, 7, 8). Taken together, the present results strongly indicate that physiological concentrations of E2 enhance insulin sensitivity, whereas high concentrations of E2 inhibit insulin-induced glucose metabolism. Part of the E2 may be converted to estrone by 17β-hydroxysteroid dehydrogenase (33). We cannot rule out the possibility that the effect of E2 is at least in part derived from estrone in 3T3-L1 adipocytes.

Treatment with E2 at any concentration did not affect the insulin-induced tyrosine phosphorylation of the insulin receptor. In contrast, the insulin-induced tyrosine phosphorylation of IRS-1, the association of IRS-1 with p85, and the phosphorylation of Akt were modulated by E2. Along with the insulin-induced glucose uptake, they were enhanced by 10^{-8} M E2 treatment and inhibited by 10^{-5} M E2 treatment. These results clearly indicate that E2 affects insulin signaling, leading to glucose uptake at least in part at the step of insulin-induced tyrosine phosphorylation of IRS-1. Although a previous report identified the decrease as the cause of 10^{-7} M E2-induced insulin resistance in 3T3-L1 adipocytes (5), 10^{-7} M E2 did not significantly affect insulin signaling, and the amount of IRS-1 was not changed by the treatment in our experiment. The difference may arise from the experimental conditions employed. In this regard, we employed fully differentiated 3T3-L1 adipocytes 14–16 d after differentiation, whereas the previous study used the cells 8–12 d after the induction of differentiation (5). By contrast, our results are consistent with reports indicating the possible mechanisms of insulin resistance in pregnant women (2, 34). Insulin-induced tyrosine phosphorylation of IRS-1 is reported to be decreased in the skeletal muscle of pregnant women compared with that in nonpregnant women (2). The reduction was even greater in pregnant women with type 2 diabetes (2). Therefore, it is possible that the effect of E2 at the level of tyrosine phosphorylation of IRS-1 is involved at least in part in the insulin resistance seen in pregnant women. It is worth noting that the cause of insulin resistance in pregnancy appears to be complex. The role of E2 in other target tissues of insulin in addition to fat cells and the roles

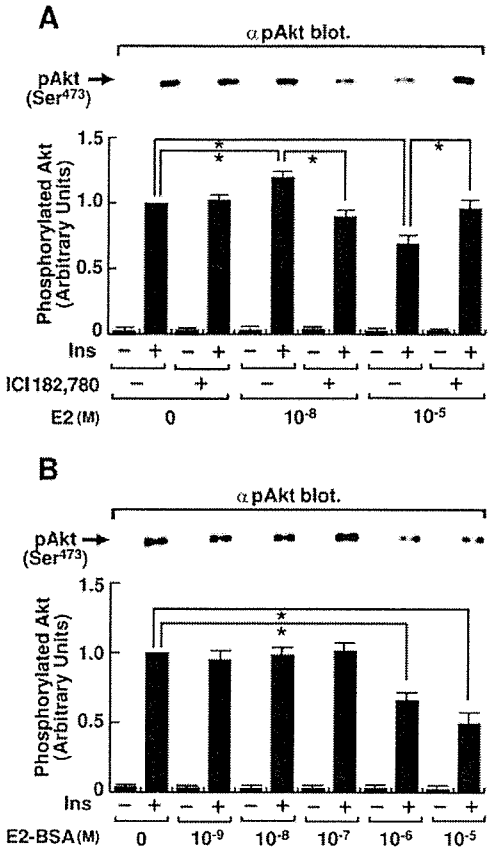

FIG. 7. Effects of ICI182,780 and E2-BSA on E2-induced alteration of insulin signaling. A, Serum-starved cells treated with 10 μM ICI182,780 and the indicated concentrations of E2 for 16 h were stimulated with 17 nM insulin for 5 min. The cell lysates were immunoblotted with antiphospho-Ser^{473}-specific Akt antibody. Results are the mean ± SE of four separate experiments. *, $P < 0.05$ *vs.* insulin-induced serine phosphorylation of Akt without ICI182,780 treatment, by ANOVA and Scheffé's test. B, Serum-starved cells treated with various concentrations of E2-BSA for 16 h were stimulated with 17 nM insulin for 5 min. The cell lysates were immunoblotted with antiphospho-Ser^{473}-specific Akt antibody. Results are the mean ± SE of four separate experiments. *, $P < 0.05$ *vs.* insulin-induced phosphorylation of Akt without E2-BSA treatment, by ANOVA and Scheffé's test.

of other hormones including progesterone need to be clarified.

Serine phosphorylation of IRS-1 is known to be a mechanism in the attenuation of insulin signaling, resulting in inhibition of tyrosine phosphorylation of IRS-1 (31). Phosphorylation of IRS-1 at Ser^{307}, Ser^{612}, and Ser^{636} is known to cause insulin resistance in 3T3-L1 adipocytes (35, 36). Interestingly, phosphorylation of IRS-1 at Ser^{307}, but not at Ser^{612} or Ser^{636}, is induced by treatment with E2 in a concentration-dependent manner. These results indicate that high concentrations of E2 inhibit insulin signaling at least in part via phosphorylation of IRS-1 at Ser^{307}. Serine 307 of IRS-1 is known to be the site of phosphorylation caused by JNK, which is a crucial mediator of insulin resistance (32). JNK1 activity is abnormally elevated in the state of insulin resistance, and an absence of JNK1 results in enhanced insulin signaling in mice and cultured cells (37). In the present study, inhibition of JNK activity by a JNK inhibitor abrogated the E2-induced inhibition of insulin-stimulated tyrosine phosphorylation of IRS-1 and serine phosphorylation of Akt. These results strengthen our idea that E2-induced JNK activation is implicated in the phosphorylation of IRS-1 at Ser^{307}, followed by inhibition of the insulin-induced tyrosine phosphorylation of IRS-1 and phosphorylation of Akt.

TNF-α is known to be a key factor causing insulin resistance by inhibiting insulin-induced tyrosine phosphorylation of IRS-1 (38, 39). Because TNF-α is also secreted from the placenta and has been implicated in insulin resistance in pregnancy, we examined the combined effects of E2 and TNF-α on insulin signaling. Because the data indicated that TNF-α combined with a submaximal concentration of E2 further inhibited insulin signaling, both agents appear to be involved in insulin resistance during late pregnancy.

ICI182,780 is known to be an antagonist of the estrogen receptor (40). Because our results showed that pretreatment with ICI182,780 abrogated the modulation of insulin-stimulated Akt phosphorylation caused by both 10^{-8} and 10^{-5} M E2, the effect of E2 on insulin signaling appears to be mediated by the estrogen receptor. Studies have revealed the existence of two receptor subtypes, estrogen receptors α and β (15, 16). Although several functional differences have been reported between these subtypes, a number of studies have demonstrated that estrogen binds to the estrogen receptor in the cytosol, and that its effect is elicited via estrogen receptors translocated to the nucleus, resulting in transcriptional activation (19–21). In addition to being located in the cytosol and, to a lesser extent, the nucleus, the estrogen receptor is known to exist on the plasma membrane (41, 42). Recent studies indicate a nontranscriptional role for the estrogen receptor in the mediation of estrogen signaling (20, 43). However, the role of estrogen receptors in the specific cellular localization during insulin signaling is totally unknown. The present study showed that membrane-impermeable E2 (E2-BSA) at 10^{-5} M inhibited the insulin-induced tyrosine phosphorylation of IRS-1 (data not shown) and serine phosphorylation of Akt, whereas they were not enhanced by E2-BSA at 10^{-8} M. These results indicate that E2's effect at high concentrations, but not at physiological concentrations, appears to be mediated by the estrogen receptors on the plasma membrane. Importantly, estrogen receptor α, but not estrogen receptor β, was redistributed upon treatment with E2. Thus, E2 at a physiological concentration (10^{-8} M) elicited the redistribution of estrogen receptor α from plasma membrane to nucleus, whereas a high concentration of E2 (10^{-5} M) induced redistribution from cytosol and nucleus to plasma membrane. Taken together, estrogen receptor α at the plasma membrane appears to be involved in the inhibitory effect of 10^{-5} M E2 on insulin signaling. The possible importance of estrogen receptor α at the plasma membrane is strengthened by the fact that E2 affects the membrane-proximal signaling of the insulin receptor located at the plasma membrane. These results are consistent with recent reports that the PI3-kinase/Akt signaling cascade is a downstream target of nonnuclear estrogenic signaling (44, 45). The lack of an effect of E2 on the cellular distribution of estrogen receptor β may be due to the low levels of estrogen receptor β in 3T3-L1 adipocytes (46).

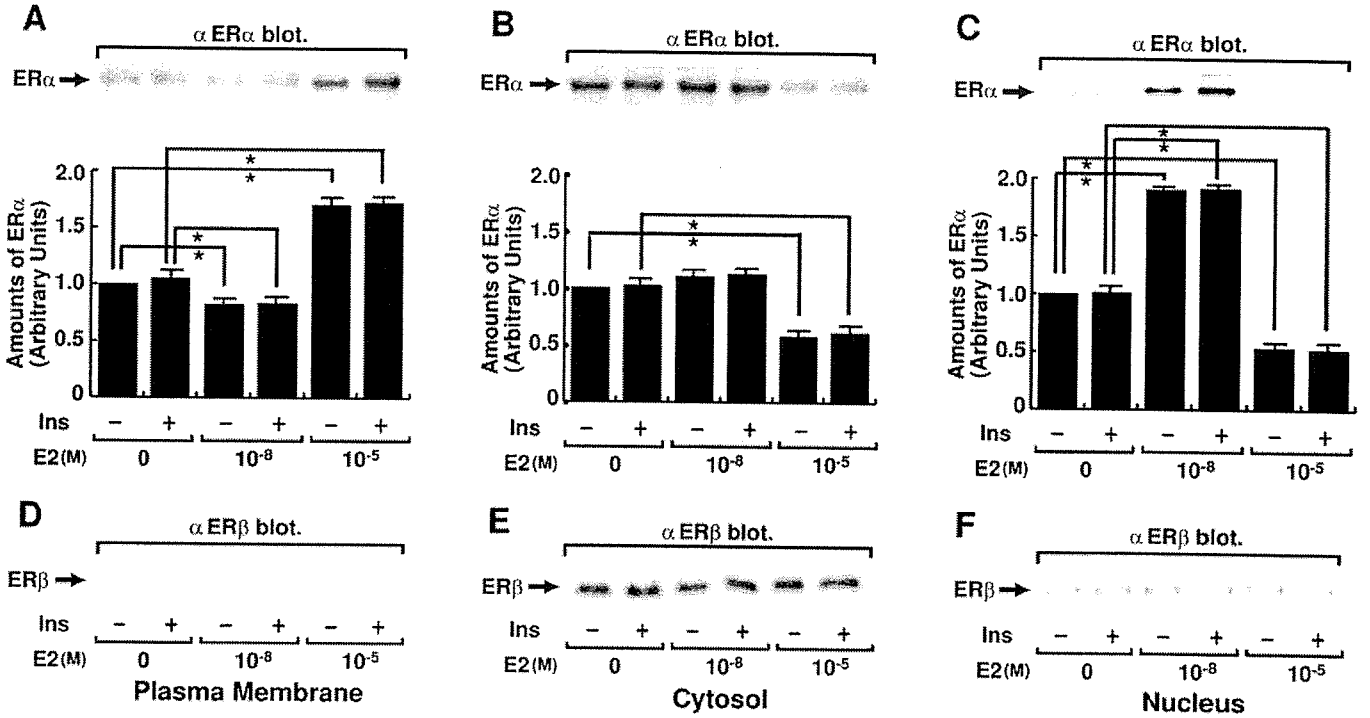

FIG. 8. Effect of E2 treatment on subcellular distribution of estrogen receptor. Serum-starved cells treated with the indicated concentrations of E2 for 16 h were stimulated without or with 17 nM insulin for 5 min. The cell lysates were fractionated into plasma membranous, cytosolic, and nuclear preparations. The samples were separated by SDS-PAGE and immunoblotted with antiestrogen receptor α antibody (αERα; A–C) or antiestrogen receptor β antibody (αERβ; D–F). Results are the mean ± SE of four separate experiments. *, $P < 0.05$ *vs.* amount of estrogen receptor α without E2 treatment, by ANOVA and Scheffé's test.

In summary, our results indicate that 1) E2 affects the metabolic action of insulin in a concentration-specific manner; 2) high concentrations of E2 inhibit insulin signaling at the level of IRS-1 by modulating the phosphorylation of IRS-1 at Ser^{307} via a JNK-dependent pathway; and 3) estrogen receptor α translocated to the plasma membrane in response to E2 is implicated in E2's inhibitory effect in 3T3-L1 adipocytes.

Acknowledgments

Received July 5, 2005. Accepted October 21, 2005.

Address all correspondence and requests for reprints to: Dr. Toshiyasu Sasaoka, Department of Clinical Pharmacology, University of Toyama, 2630 Sugitani, Toyama, 930-0194, Japan. E-mail: tsasaoka-tym@umin.ac.jp.

This work was supported in part by a Grant-in-Aid for Scientific Research from the Japan Society for the Promotion of Science (to T.S., M.K., and S.S.); the 21st Century Center of Excellence (COE) program from the Ministry of Education, Culture, Sports, Science, and Technology of Japan (to S.S.); and a grant for Research on Sensory and Communicative Disorders from the Ministry of Health, Labor, and Welfare, Japan (to T.S.).

References

1. **Yamashita H, Shao J, Friedman JE** 2000 Physiologic and molecular alterations in carbohydrate metabolism during pregnancy and gestational diabetes mellitus. Clin Obstet Gynecol 43:87–98
2. **Friedman JE, Ishizuka T, Shao J, Huston L, Highman T, Catalano P** 1999 Impaired glucose transport and insulin receptor tyrosine phosphorylation in skeletal muscle from obese women with gestational diabetes. Diabetes 49: 1807–1814
3. **Ryan EA, O'Sullivan MJ, Skylar JS** 1985 Insulin action during pregnancy: studies with the euglycemic clamp technique. Diabetes 34:380–389
4. **Ryan EA, Enns L** 1988 Role of gestational hormones in the induction of insulin resistance. J Clin Endocrinol Metab 67:341–347
5. **Collison M, Campbell IW, Salt IP, Dominiczak AF, Connell JMC, Lyall H, Gould GW** 2000 Sex hormones induce insulin resistance in 3T3–L1 adipocytes by reducing cellular content of IRS proteins. Diabetologia 43:1374–1380
6. **Kirwan JP, Haugel-de Mouzon S, Lepercq J, Challier J-C, Huston-Presley L, Friedman JE, Kalhan SC, Catalano PM** 2002 TNF-α is a predictor of insulin resistance in human pregnancy. Diabetes 51:2207–2213
7. **Brussaard HE, Gevers-Leuven JA, Flölich M, Kluft C, Krans HMJ** 1997 Short-term oestrogen replacement therapy improves insulin resistance, lipids and fibrinolysis in postmenopausal women with NIDDM. Diabetologia 40: 843–849
8. **Hernandez-Ono A, Monter-Carreola G, Zamora-Gonzalez J, Cardoso-Saldana G, Posadas-Sanchez R, Torres-Tamayo M, Posadas-Romero C** 2002 Association of visceral fat with coronary risk factors in a population-based sample of postmenopausal women. Int J Obes Relat Metab Disord 26:33–39
9. **Brochu M, Starling RD, Tchernof A, Matthews DE, Garcia-Rubi E, Poehlman ET** 2000 Visceral adipose tissue is an independent correlate of glucose disposal in older obese postmenopausal women. J Clin Endocrinol Metab 85:2378–2384
10. **Inoue G, Cheatham B, Emkey R, Kahn CR** 1998 Dynamics of insulin signaling in 3T3–L1 adipocytes: differential compartmentalization and trafficking of insulin receptor substrate (IRS)-1 and IRS-2. J Biol Chem 273:11548–11555
11. **Czech MP, Corvera S** 1999 Signaling mechanisms that regulate glucose transport. J Biol Chem 274:1865–1868
12. **Saltiel AR, Kahn CR** 2001 Insulin signalling and the regulation of glucose and lipid metabolism. Nature 414:799–806
13. **Virkamäki A, Ueki K, Kahn CR** 1999 Protein-protein interaction in insulin signaling and the molecular mechanisms of insulin resistance. J Clin Invest 103:931–943
14. **Alessi DR, Andjelkovic M, Caudwell B, Cron P, Morrice N, Cohen P, Hemmings BA** 1996 Mechanism of activation of protein kinase B by insulin and IGF-1. EMBO J 15:6541–6551
15. **Green S, Walter P, Kumar V, Krust A, Bornert JM, Argos P, Chambon P** 1986 Human oestrogen receptor cDNA: sequence, expression and homology to v-*erb*-A. Nature 320:134–139
16. **Kuiper GGJM, Enmark E, Pelto-Huikko M, Nilsson S, Gustafsson J-A** 1996

Cloning of a novel estrogen receptor expressed in rat prostate and ovary. Proc Natl Acad Sci USA 93:5925–5930
17. **Enmark E, Gustafsson J-A** 1999 Oestrogen receptors–an overview. J Intern Med 246:133–138
18. **Mendelsohn ME** 2002 Protective effects of estrogen on the cardiovascular system. Am J Cardiol 89(Suppl):12E–18E
19. **Hager GL, Lim CS, Elbi C, Baumann CT** 2000 Trafficking of nuclear receptors in living cells. J Steroid Biochem Mol Biol 74:249–254
20. **Moss RL, Gu Q, Wong M** 1997 Estrogen nontranscriptional signaling pathway. Rec Prog Horm Res 52:33–70
21. **Pappas TC, Gametchu B, Watson CS** 1995 Membrane estrogen receptors identified by multiple antibody labeling and impeded-ligand binding. FASEB J 9:404–410
22. **Kitamura T, Ogawa W, Sakaue H, Hino Y, Kuroda S, Tanaka M, Matsumoto M, Maeda T, Konishi H, Kikkawa U, Kasuga M** 1998 Requirement for activation of the serine-threonine kinase Akt (protein kinase B) in insulin stimulation of protein synthesis but not of glucose transport. Mol Cell Biol 18: 3708–3717
23. **Ueki K, Yamamoto-Honda R, Kaburagi Y, Yamauchi T, Tobe K, Burgering BMT, Coffer PJ, Komuro I, Akanuma Y, Yazaki Y, Kadowaki T** 1998 Potential role of protein kinase B in insulin-induced glucose transport, glycogen synthesis, and protein synthesis. J Biol Chem 273:5315–5322
24. **Takano A, Usui I, Haruta T, Kawahara J, Uno T, Iwata M, Kobayashi M** 2001 Mammalian target of rapamycin pathway regulates insulin signaling via subcellular redistribution of insulin receptor substrate 1 and integrates nutritional signals and metabolic signals of insulin. Mol Cell Biol 21:5050–5062
25. **Ishihara H, Sasaoka T, Hori H, Wada T, Hirai H, Haruta T, Langlois WJ, Kobayashi M** 1999 Molecular cloning of rat SH2-containing inositol phosphatase 2 (SHIP2) and its role in the regulation of insulin signaling. Biochem Biophys Res Commun 260:265–272
26. **Wada T, Sasaoka T, Funaki M, Hori H, Murakami S, Ishiki M, Haruta T, Asano T, Ogawa W, Ishihara H, Kobayashi M** 2001 Overexpression of SH2-containing inositol phosphatase 2 results in negative regulation of insulin-induced metabolic actions in 3T3–L1 adipocytes via its 5′-phosphatase catalytic activity. Mol Cell Biol 21:1633–1646
27. **Burgering BM, Coffer PJ** 1995 Protein kinase B (c-Akt) in phosphatidylinositol-3-OH kinase signal transduction. Nature 376:599–602
28. **Cong L-N, Chen H, Li Y, Zhou L, McGibbon MA, Taylor SI, Quon MJ** 1997 Physiological role of Akt in insulin-stimulated translocation of GLUT4 in transfected rat adipose cells. Mol Endocrinol 11:1881–1890
29. **Chen HL, Yang YP, Hu XL, Yelavarthi KK, Fishback JL, Hunt JS** 1991 Tumor necrosis factor α mRNA and protein are present in human placental and uterine cells at early and late stages of gestation. Am J Pathol 139:327–335
30. **Innes KE, Wimsatt JH, McDuffie R** 2001 Relative glucose tolerance and subsequent development of hypertension in pregnancy. Obstet Gynecol 97: 905–910
31. **Aguirre V, Werner ED, Giraud J, Lee YH, Shoelson SE, White MF** 2002 Phosphorylation of Ser^{307} in insulin receptor substrate-1 blocks interactions with the insulin receptor and inhibits insulin action. J Biol Chem 277:1531–1537
32. **Aguirre V, Uchida T, Yenush L, Davis R, White MF** 2000 The c-Jun NH_2-terminal kinase promotes insulin resistance during association with insulin receptor substrate-1 and phosphorylation of Ser^{307}. J Biol Chem 275:9047–9054
33. **Corbould AM, Judd SJ, Rodgers RJ** 1998 Expression of types 1, 2, and 3 17β-hydroxysteroid dehydrogenase in subcutaneous abdominal and intra-abdominal adipose tissue of women. J Clin Endocrinol Metab 83:187–194
34. **Shao J, Catalano PM, Yamashita H, Ruyter I, Smith S, Youngren J, Friedman JE** 2000 Decreased insulin receptor tyrosine kinase activity and plasma cell membrane glycoprotein-1 overexpression in skeletal muscle from obese women with gestational diabetes mellitus (GDM): evidence for increased serine/threonine phosphorylation in pregnancy and GDM. Diabetes 49:603–610
35. **Rui L, Aguirre V, Kim JK, Shulman GI, Lee A, Corbould A, Dunaif A, White MF** 2001 Insulin/IGF-1 and TNF-α stimulate phosphorylation of IRS-1 at inhibitory Ser^{307} via distinct pathways. J Clin Invest 107:181–189
36. **Gual P, Gremeaux T, Gonzalez T, Le Marchand-Brustel Y, Tanti J-F** 2003 MAP kinases and mTOR mediate insulin-induced phosphorylation of insulin receptor substrate-1 on serine residues 307, 612, and 632. Diabetologia 46: 1532–1542
37. **Hirosumi J, Tuncman G, Chang L, Görgün CZ, Uysal KT, Maeda K, Karin M, Hotamisligil GS** 2002 A central role for JNK in obesity and insulin resistance. Nature 420:333–336
38. **Peraldi P, Hotamisligil GS, Buurman WA, White MF, Spiegelman BM** 1996 Tumor necrosis factor (TNF)-α inhibits insulin signaling through stimulation of the p55 TNF receptor and activation of sphingomyelinase. J Biol Chem 271:13018–13022
39. **Hotamisligil GS, Peraldi P, Budavari A, Ellis R, White MF, Spiegelman BM** 1996 IRS-1-mediated inhibition of insulin receptor tyrosine kinase activity in TNF-α and obesity-induced insulin resistance. Science 271:665–668
40. **Wakeling AE, Dukes M, Bowler J** 1991 A potent specific pure antiestrogen with clinical potential. Cancer Res 51:3867–3873
41. **Pietras RJ, Nemere I, Szego CM** 2001 Steroid hormone receptors in target cell membranes. Endocrine 14:417–427
42. **Ho KJ, Liao JK** 2002 Nonnuclear actions of estrogen. Arterioscler Thromb Vasc Biol 22:1952–1961
43. **Razandi M, Pedram A, Greene GL, Levin ER** 1999 Cell membrane and nuclear estrogen receptors (ERs) originate from a single transcript: studies of ERα and ERβ expressed in Chinese hamster ovary cells. Mol Endocrinol 13:307–319
44. **Simoncini T, Hafezi-Moghadam A, Brazil DP, Ley K, Chin WW, Liao JK** 2000 Interaction of oestrogen receptor with the regulatory subunit of phosphatidylinositol-3-OH kinase. Nature 407:538–541
45. **Simoncini T, Rabkin E, Liao JK** 2003 Molecular basis of cell membrane estrogen receptor interaction with phosphatidylinositol 3-kinase in endothelial cells. Arterioscler Thromb Vasc Biol 23:198–203
46. **Rodriguez-Cuenca S, Monjo M, Proenza AM, Roca P** 2005 Depot differences in steroid receptor expression in adipose tissue: possible role of the local steroid milieu. Am J Physiol 288:E200–E207

Endocrinology is published monthly by The Endocrine Society (http://www.endo-society.org), the foremost professional society serving the endocrine community.

Current Eye Research, 31:947–953, 2006

ISSN: 0271-3683 print / 1460-2202 online
DOI: 10.1080/02713680600966785

informa
healthcare

Induction of Endoplasmic Reticulum Stress in Retinal Pericytes by Glucose Deprivation

Kengo Ikesugi,
Michael L. Mulhern,
and Christian J. Madson
Department of Ophthalmology & Visual Sciences, University of Nebraska Medical Center, Omaha, Nebraska, USA

Ken-ichi Hosoya
Faculty of Pharmaceutical Sciences, Toyama Medical and Pharmaceutical University, Toyama, Japan

Tetsuya Terasaki
Department of Molecular Biopharmacy and Genetics, Graduate School of Pharmaceutical Sciences, Tohoku University, Sendai, Japan

Peter F. Kador
College of Pharmacy, University of Nebraska Medical Center, Omaha, Nebraska, USA

Toshimichi Shinohara
Department of Ophthalmology & Visual Sciences, University of Nebraska Medical Center, Omaha, Nebraska, USA

Received 24 October 2005
Accepted 15 August 2006

Correspondence: Toshimichi Shinohara, Ph.D., Professor of Ophthalmology and Visual Sciences, University of Nebraska Medical Center, 985840 Nebraska Medical Center, Omaha, NE 68198-5840, USA. E-mail: shinoharalab@hotmail.com

ABSTRACT Diabetic retinopathy is one of the major microvascular complications associated with diabetes mellitus, and the selective degeneration of retinal capillary pericytes is considered to be a hallmark of early retinopathy. Because glucose fluctuations commonly occur in diabetes, we hypothesized that these fluctuations will increase the endoplasmic reticulum (ER) stress and induce the unfolded protein response (UPR) in retinal pericytes. To study whether ER stress and the UPR can be induced in retinal pericytes, rat retinal capillary pericytes were cultured in different concentrations of glucose. Hypoglycemia but not hyperglycemia was found to activate UPR-specific enzymes in pericytes. Strong UPR activation leading to apoptosis was also observed when pericytes were cultured in glucose concentrations that were reduced from high to low or no glucose. These results indicate that induction of UPR is related not only to absolute concentrations but also to a shifting from higher to lower concentrations of glucose.

KEYWORDS apoptosis; diabetic retinopathy; endoplasmic reticulum (ER) stress; retinal pericytes; unfolded protein response (UPR)

INTRODUCTION

The incidence of diabetes mellitus has significantly increased in recent years, and poor control of this disease leads to a number of systemic and ocular complications. Diabetic retinopathy is a major microvascular complication of diabetes, and its proliferative stage is a leading cause of blindness.

Retinal capillaries are composed of pericytes and endothelial cells. Pericytes provide vascular stability, and their selective loss is a hallmark of early microvascular lesions.[1–3] Pericytes do not replicate in the adult retina, and their degeneration leads to basement membrane thickening, increased vascular permeability, and retinal edema.[4] The loss of pericytes can also result in focal retinal capillary endothelial cell proliferation leading to microaneurysms[5] or to degeneration of endothelial cells to form acellular capillaries, which can lead to a subsequent formation of areas of nonperfusion.

Animal models have played a critical role in elucidating the pathologic mechanisms associated with the clinical lesions of diabetic retinopathy. Extensive studies have been conducted using diabetic rats. Absent to date have been *in vitro* studies using cultures of rat retinal capillary cells. Studies have mainly

used bovine pericytes, presumably because of difficulties in preparing rat retinal pericytes in adequate amounts and purity. Recently, however, a cell line of rat retinal capillary pericytes (TR-rPCT) has been established from a transgenic rat harboring the temperature-sensitive simian virus 40 (SV 40) large T-antigen gene (Tg rat).[6] Use of this cell line allows for direct biochemical comparisons and correlations between *in vitro* and *in vivo* results.

Recently, the endoplasmic reticulum (ER) has been recognized to play a pivotal role in the progression of many human diseases.[7] Unfolded protein aggregates in the ER induce ER stress, which then generates the unfolded protein response (UPR). Upon activation, the UPR initiates diverse signaling responses. Under normal conditions, this coordinated response halts the buildup of proteins, allows time for the elimination of unfolded proteins, and reestablishes cellular homeostasis. However, a prolongation of the UPR induces apoptosis.[7] The UPR was initially observed in diseases such as Alzheimer disease and Parkinson disease, which are characterized by the accumulation of misfolded mutant protein aggregates.[8] More recently, obesity has been reported to induce UPR, and this may be associated with a diabetes-induced imbalance of glucose.[9,10]

Because UPR signaling has been shown to be essential for the maintenance of glucose homeostasis, it is hypothesized that the ER stress–UPR system may also affect retinal pericyte viability and function. Glucose fluctuations in patients with diabetes mellitus could initiate ER stress that generates a UPR that, if unalleviated, could lead to apoptosis of retinal pericytes. In this report, we present evidence that glucose deprivation, a known ER stressor, and rapid reduction of glucose levels induce the UPR in cultured retinal pericytes. This suggests a link between ER stress and apoptosis of retinal pericytes. Moreover, these findings may provide insight into the clinical observation that establishment of tight control in diabetics, which is associated with increased incidences of hypoglycemia, is initially accompanied by an acceleration of retinopathy.

MATERIALS AND METHODS

Cell Culture

Conditionally immortalized rat retinal pericytes (TR-rPCT)[6] were cultured on collagen type 1 coated plates or dishes in a normal glucose (5.5 mM) Dulbecco'sModified Eagle's Medium (DMEM; Invitrogen-Gibco, Grand Island, NY, USA) supplemented with 10% heat-inactivated fetal bovine serum (FBS), 100 μg/ml streptomycin, and 100 U/ml penicillin in a 6% CO_2 atmosphere at 33°C. The cells were released from the plates with trypsin in phosphate-buffered saline (PBS) containing 1 mM EDTA-Na and plated at a density of 2×10^4 in 96-well plates, 1×10^5 in 24-well plates, or 2×10^6 in 100-mm dishes depending on the experiment. After an overnight incubation, the attached pericytes were washed twice and incubated with serum-free DMEM containing specified concentrations of glucose for specific times.

Cell Viability Assay

A colorimetric assay was performed using the CellTiter 96 AQueous One Solution Cell Proliferation Assay kit (Promega, Madison, WI, USA) according to the manufacturer's protocol. This colorimetric assay of cellular proliferation uses 3-(4,5-dimethylthiazol-2-yl)-5-(3-carboxy-methoxyphenyl)-2 to 4-sulfophenyl)-2H-tetrazolium salt (MTS). When MTS is added to a medium containing living cells, it is reduced to a water-soluble formazan salt, and the quantity of formazan is directly proportional to the number of living cells. The absorbance of formazan was measured at 490 nm with an ELISA plate reader 1 hr after the addition of MTS.

TUNEL Staining

TdT-mediated dUTP-biotin nick end labeling (TUNEL) staining was carried out using a fluorescein *in situ* cell death detection kit (Roche Diagnostics, Mannheim, Germany) according to the manufacturer's protocol. Briefly, cells were washed with PBS and fixed in freshly prepared 4% paraformaldehyde in PBS. This was followed by a 2-min incubation with ice-cold permeabilization solution (0.1% Triton X-100, 0.1% sodium citrate). The cells were then rinsed twice with PBS and incubated for 1 hr at 37°C with the TUNEL reaction mixture. After incubation, the cells were rinsed three times with PBS, mounted on microscope slides, and photographed using a fluorescent microscope (Nikon Instruments Inc., Melville, NY, USA). The percentage of apoptotic cells/total cells (100 cells) in